Alma Mater Studiorum – Università di Bologna

DOTTORATO DI RICERCA IN

**Chimica Industriale**

Ciclo XXV

Settore Concorsuale di afferenza: **03/C2**

Settore Scientifico disciplinare: **CHIM/04**

# Investigation of heterogeneous catalysts

# for the synthesis of fine chemicals

Presentata da
**Alessandra Giugni**

| Coordinatore Dottorato | Relatore |
|---|---|
| **Prof. Fabrizio Cavani** | **Chiar. mo Prof. Angelo Vaccari** |
| | Correlatore |
| | **Dott. Carlo Lucarelli** |

**Esame finale anno 2013**

# Abstract

In order to match the more stringent environmental regulations, heterogenization of traditional homogeneous processes is one of the main challenges of the modern chemical industry. Great results have been achieved in the fields of petrochemicals and base chemicals, whereas in fine chemical industry most of the synthetic procedures are based on multistep processes catalyzed by homogeneous catalysts mainly used in stoichiometric amounts. In the fine chemicals manufacture not so much efforts have been devoted to the investigation of suitable solid catalysts for the development of greener processes, then this sector represent a very attractive field of research. In this context, the present work deals with the extensive investigation of the possibility to heterogenize existing processes, in particular two different classes of reactions have been studied: alkylation of aromatic and heteroaromatic compounds and selective oxidation of aromatic alcohols. Traditional solid acid catalysts, such as zeolites, clays and alumina have been tested in the gas phase alkylation of 1,2-methylendioxybenzene, core building block of many drugs, pesticides and fragrances. The observed reactivity were clarified through a deep FTIR investigation complemented by ab initio calculation. The same catalysts were tested in the gas phase isopropylation of thiophene with the aim of clearly attribute the role of the reaction parameters in the reaction proceeding and verify the possibility to enhance the selectivity of one of the two possible isomers. Finally various $Au/CeO_2$ catalysts were tested in the synthesis of benzaldehyde and piperonal, two aldehydes largely employed in the manufacture of fine chemical products, through liquid phase oxidation of the corresponding alcohols in very mild conditions.

# Index

II

# Chapter 1

# Spectroscopic evidence for 1,2-methylendioxybenzene inertia in heterogeneous catalytic systems[1]

## INTRODUCTION

Alkylation of aromatic hydrocarbons is one of the most useful reactions in organic chemistry for the synthesis of petrochemicals, intermediates, and fine chemical products.[2] The high costs in terms of product purification and toxic waste disposal make it imperative for research to develop new processes based on solid catalysts. Petrochemical traditional reactions have been replaced with new ones based on solid-acid catalysts:[3,4] benzene, toluene, biphenyl, and naphthalene alkylations[5–11] may be cited as examples. In the field of fine chemicals, most of the current processes are still based on homogeneous catalysts.[3,12] 5-Substituted benzo[1,3]dioxole derivatives are important compounds in the manufacture of fragrances (Piperonal, Helional), drugs (Tadafil, Anolignan A, etc.), and agrochemicals (Piperonyl Butoxide).[13–16]

In this work, the attention was first focused on Helional (3-[3,4-methylendioxyphenyl]-2-methyl-propionaldehyde), whose synthesis starting from 1,2-methylenedioxybenzene (MDB) is industrially carried out in the liquid phase, using Lewis acid catalysts and operating in batch conditions. Traditional synthetic procedures are based on a two steps process: (i) alkylation of aromatic substrate with the suitable alkenylidenediacetate and (ii) hydrolysis of the obtained precursor to the desired product. In case of Helional, MDB is alkylated by 2-methylprop-2-ene-1,1-diyl diacetate yielding 1-acetoxy-2-methyl-3-(3,4-methylendioxyphenyl) propene), which is hydrolyzed to the corresponding aldehyde, Scheme 1. The

described processes are generally carried out in the liquid phase by using homogeneous catalytic systems such as $TiCl_4$ and $AlCl_3$, metal halides or boron trifluoride-diethylether complexes. [17–20]



1-acetoxy-2-methyl-3-
(3,4-methylendioxyphenyl)propene

Helional

Scheme 1
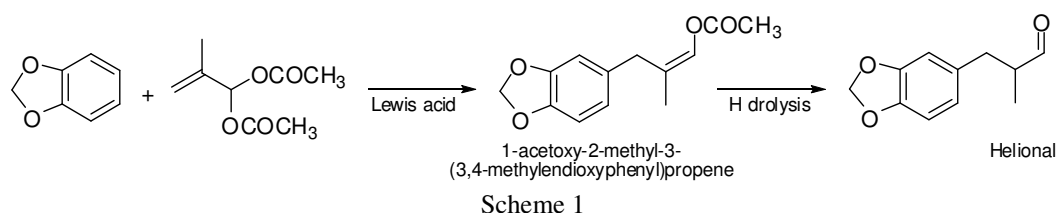
Several authors have suggested some alternative routes for the synthesis of 5-alkylbenzo[1,3]dioxole avoiding the alkylation of MDB. In particular, Borzatta *et al.*[21,22] described two multi-step processes starting from the acylation of MDB or from 4-acylphenol, whereas Zelle *et al.*[23] described one process starting from the reaction of 4-alkyl-catechols with methylene dihalide.

A review of the literature[4,5,7,8,12] shows that heterogeneously catalyzed alkylations of aromatic hydrocarbons are important reactions and have been studied in depth in recent years, with the most studied reactions being the alkylation of benzene and alkyl-substituted benzene. Conversely, for oxygen-containing benzene derivatives very few data on the reactivity with heterogeneous catalytic systems are available, thus suggesting that in this case the reaction is much more demanding. Considering MDB, the only example of heterogeneous reaction is the acetylation reported by Spagnol et al.[24] in the presence of beta zeolite carried out batchwise with a 61% yield. A detailed look at the step by-step process through which the reaction occurs may be an interesting way to verify the effective feasibility of the alkylation.

Spectroscopic techniques have been widely used to study the alkylation of benzene or alkylbenzene derivatives with different alkylating agents (methanol, ethylene, propylene, 2-propanol, etc.) on solid-acid catalyst such as zeolite. Furthermore infrared spectroscopic studies of adsorption of various probe molecules (such as benzene, pyridine, THF, and methanol) have been successfully used to investigate the acidic properties of zeolite, thus nature of the acid sites is unanimously recognized.[25–27] A number of papers have been published on the interaction between aromatic substrates and the catalyst surface, but some debate still exists. The interaction of different classes of aromatic hydrocarbons, such as benzene and toluene, with the protonic sites of zeolites has been studied using IR spectroscopy. In the above mentioned papers the attention has mainly been focused on the interaction between the molecule and the acid sites, leading to the evaluation of their nature and location, without considering the evolution of the properties of aromatic ring.[28–33] Nevertheless, the activation and reactivity of different alkylating agents such as methyl, propyl, etc. on zeolite catalysts are well known today.[34–40]

The aim of this work is to clarify the catalytic behavior of complex aromatic substrates through the investigation, using FT-IR spectroscopy, of the nature of the

interaction with the catalyst surface. The experimental IR spectra were complemented with ab initio calculations of the IR frequencies to help the assignment of the bands.

# EXPERIMENTAL

*Materials.* 1,2-Methylendioxybenzene (MDB) (99%), 1,2-ethylendioxybenzene (EDB) (97% wt.%), 1,2-dimethoxybenzene (DEB) (99% wt.%), acrolein diethyl acetal (AEA) (96% wt.%), 2-propanol (99.5% ), 1-bromopropane (99%), sulfuric acid (96%), anhydrous aluminum chloride (≥99.9%), anhydrous sodium sulfate (≥99.0%), dichloromethane (≥99.9%) were purchased from Aldrich Chemicals and used without any further purification.

Different commercial solid-acid catalysts have been studied such as $\gamma$-$Al_2O_3$ (Sasol), acid-treated clay (Engelhard, F-13), and a beta zeolite (Zeocat PB). Before the tests all the samples were calcined at 500°C for 6 hours.

*Catalytic tests.*

    *Heterogeneous gas phase tests.* The heterogeneous gas phase catalytic tests were carried out at atmospheric pressure in a fixed bed continuous-flow reactor (length 390 mm and inner diameter 8 mm) at 300 °C using $N_2$ as the carrier gas. The reactor was charged with 1 cm$^3$ (particle size 40-60 mesh) of fresh catalyst. Aromatic substrates (MDB, EDB, and DEB) were fed in excess to the alkylating agents (acrolein diethyl acetal or 2-propanol) in a molar ratio of 3. The reaction mixture was fed using a syringe pump and vaporized into a preheated flow of $N_2$, set to reach a 9:1 volume ratio of $N_2$ to organic mixture (aromatic substrate and alkylating agent). All runs were performed at a contact time of 1s. During the catalytic tests the outlet stream was condensed in HPLC-grade acetone, and cooled in an ice bath at 0°C for 1h. Blank tests, without a catalyst, at the same reaction temperature did not show any reaction and/or decomposition.

    *Heterogeneous liquid phase tests.* Liquid phase heterogeneously catalyzed tests were conducted in a glass batch reactor equipped with reflux condenser, by reacting 2.5 mmol of aromatic substrate in 5 ml of 2-propanol with 0.1 mg of catalyst at boiling temperature of the alchool for 2 hours. The obtained mixture was filtered before the analysis.

    *Homogeneous liquid phase tests.* Two different procedures were employed in the homogeneous tests: 1) 49.0 mmol of aromatic substrate were added to 3.0 mmol of anhydrous aluminum chloride. Then 49.0 mmol of 1-bromopropane were added dropwise, keeping the mixture under stirring for 30 minutes at 40 °C. 5 ml of cold water were added to the solution then organic phase was diluted with $CH_2Cl_2$ and dried with anhydrous sodium sulfate before analysis; 2) 2.2 mmol of aromatic substrate were mixed with 0.5 ml of 2-propanol then 1 ml of sulfuric acid was added dropwise keeping the solution into an ice bath. Afterwards, the mixture was

allowed to warm at room temperature and the reaction was pursued for further 10 minutes. Then, a procedure similar to that previously described for AlCl$_3$ was followed before the analysis.

All the obtained solutions were analyzed using a Carlo Erba 4300 gas chromatograph, equipped with FID and a wide-bore OV1 column (length 30 m, i.d. 0.53 mm, film width 0.5 µm) and identified by GC-MS analysis using an Agilent Technology 6890N equipped with a 5973 mass selective detector and an HP5 column (length 25 m, i.d. 0.25 mm, film width 1.5 µm).

*IR studies*. The IR spectra after adsorption of reactants were recorded using a Perkin Elmer Spectrum One spectrometer. Zeolite and alumina samples were pressed into self-supported wafer and activated in situ in the IR cell at 500°C under a vacuum ($\leq$ 10-7 mbar) for 1 h. Before measuring the IR spectra, the activated sample was contacted with an increasing amount of the adsorbent at room temperature. Desorption spectra were recorded at temperature increasing from room to 500°C. For recording spectra, 12 scans were co-added with a resolution of 1 cm$^{-1}$ in the region of 4000-450 cm$^{-1}$.

*Computational calculation.* IR frequencies of MDB, EDB, and DEB molecules were calculated at the MP2(FC) level using the 6311G(d,p) basis set by the Gaussian09 software package.[41] IR frequencies were scaled by a factor of 0.9496.[42]

*Characterization.* Ammonia-Temperature Programme Desorption (NH$_3$-TPD). Acid properties of the catalysts have been evaluated by means of temperature programmed desorption (TPD) of NH$_3$ using a Termoquest TPDRO instrument. Approximately 120 mg of the catalyst sample were pretreated in He flow (20 ml/min) at 500 °C for 1 h. The sample was then cooled to 200 °C and flushed with 10% NH$_3$/He (20 ml/min) until saturation. Physically adsorbed NH$_3$ was eliminate purging the sample with He (20 ml/min) for 30 minutes. The sample was then heated to 500 °C at a rate of 10 °C/min, simultaneously NH$_3$ desorption was continuously monitored by TCD detector.

## RESULTS AND DISCUSSION

The work may be divided in two parts: (i) investigation of the MDB reactivity in alkylation reactions catalyzed by both heterogeneous and homogeneous catalysts followed by a comparison with the reactivity of EDB and DEB under the same conditions, and (ii) FTIR studies on the nature of the interaction between the molecule and the catalytic sites, supported by ab intio calculations, and effect on the reactivity.

## Catalytic tests

The alkylation of MDB with 3-diacetoxy-2-methylpropene gives 1-acetoxy-2-methyl-3-(3,4-methylendioxyphenyl) propene (precursor of Helional), which can be easily hydrolyzed to the desired aldehyde, Helional (Scheme 1). In the present work the gas phase alkylation of MDB was studied using acrolein diethyl acetal (AEA) as a commercially available model of 3-diacetoxy-2-methylpropene (Scheme 2).
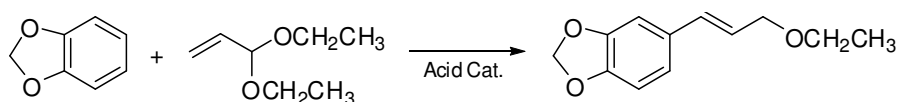


Scheme 2

Three solid catalysts with different acid-base properties were tested at 300°C: $\gamma$-Al$_2$O$_3$, acid-treated clay (Engelhard F-13), and beta zeolite (HBEA, Zeocat PB) (Table 1).

Table 1. Acidity and activity of the tested samples at 300°C.

| catalyst | acid amount (mmol NH$_3$/g$_{cat}$) | AEA conv (%) | MDB conv (%) | yield (%) |
|---|---|---|---|---|
| $\gamma$-Al$_2$O$_3$ | 0.05 | 35 | 10 | 0 |
| F-13 | 0.4 | 85 | 14 | 0 |
| H-BEA | 0.5 | 90 | 9 | 0 |

GC-MS analysis of the condensed outlet stream does not show the formation of any products. The conversion of AEA is mostly due to its decomposition (to acetaldehyde, ethanol, propanal, 1-propene-3-ethoxy, ethyl-1-propenyl ether) and heavy byproducts formation. MDB is involved only in undesired reactions yielding heavy byproducts, which remain adsorbed on the catalyst surface.

These results may be explained by two phenomena: i) AEA totally decomposes before reacting with the aromatic substrate; ii) MDB is not reactive in the tested conditions. In order to verify the first hypothesis, AEA reactivity was studied in the 140-350 °C range, feeding 0.75 ml/h of AEA in a preheated flow (20 ml/min) of N$_2$ on a beta zeolite sample. The results show that the compound decomposes from about 20 to 100% throughout the whole temperature range investigated. In particular when operating at 300 °C the reactant totally decomposes within the first hour, the decomposition decreases with time on stream due to catalyst deactivation by coke formation. Thus, at operating conditions, this molecule is not stable enough to alkylate an aromatic substrate. Then the alkylation of MDB was studied using 2-propanol, a more stable alkylating agent, whose activity has been studied in depth in gas phase aromatic alkylation.[6,7,43] For the sake of comparison the same reaction

was carried out on ethylendioxy and dimethoxy-substituted benzene derivatives, 1,2-ethylendioxybenzene (EDB) and 1,2-dimethoxybenzene (DEB), Scheme 3.



Scheme 3
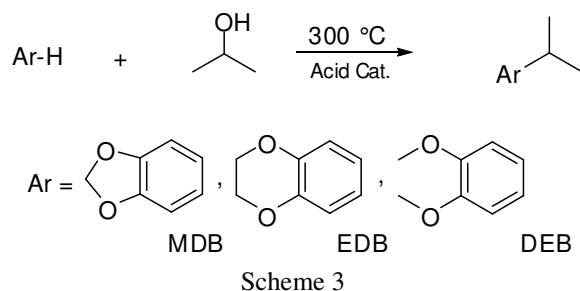
Tests were conducted over zeolite BEA, γ-alumina and acid treated clay samples. MDB shows a conversion lower than 10% and no evidence of products formation over all the catalysts investigated; while EDB readily reacts (conversion from 60% to 70%) with 2-propanol to give monoalkylated products which undergo further polyalkylation to di- and tri-isopropyl-EDB; the products distribution depends on the acidity of the tested catalyst. Finally, in the case of DEB the reaction (conversion ~ 90% for all the catalysts) leads to the formation of mono- and dialkylated derivatives which undergo Fries rearrangement[44] to yield a very complex products mixture.

In order to understand if the above reported results are due to the heterogeneity of catalytic system or to operating conditions (gas or liquid phase) similar tests were performed in liquid phase, both in heterogeneous (alumina and zeolite) and homogeneous systems (AlCl$_3$ and H$_2$SO$_4$). In the former case, MDB is totally unreactive, while EDB reaches conversions of 43 and 29% using zeolite and alumina respectively; DEB shows higher conversion (52 and 38%) with the formation of mono- and dialkylated products.

The tests performed using homogeneous catalysts show different results: as expected, EDB and DEB are highly reactive, reaching conversion values between 70 and 80%, with good selectivity values in monoalkylated products. MDB shows a completely different reactivity compared to the tests with the heterogeneous catalysts. In fact for both homogeneous investigated catalysts, a conversion of about 40% is obtained, with formation of mono- and dialkylated products.

Summarizing (Table 2), the three considered molecules show a good reactivity in well-known homogeneous conditions, while only MDB is totally unreactive on solid acidic catalysts. Then the different behaviors in heterogeneous catalysis between the substrates studied may be caused by the geometric conformation of the molecules, which causes a different interaction of the benzene moiety with the catalyst surface. In order to verify this hypothesis the conformational properties of MDB, EDB and DEB were studied and geometry optimizations were carried out.

Table 2. Schematic summary of the results obtained in the performed catalytic tests.

| Gas Phase Tests |
| --- |
| *Gas Phase Tests (, γ-Al$_2$O$_3$, F-13 and HBEA)* |
| **MDB conv < 10% and no products formation** |
| EDB conv 60-70% mono and dialkylated products |
| DEB conv > 90% complex mixture of products |
| (Fries rearrangement and alkylation) |
| |
| **Liquid phase tests** |
| *Heterogeneous catalytic systems (γ-Al$_2$O$_3$ HBEA)* |
| **MDB totally unreactive** |
| EDB conv 43% (γ-Al$_2$O$_3$) 29% (HBEA) |
| DEB conv 52% (γ-Al$_2$O$_3$) 38% (HBEA) |
| |
| *Homogeneous catalytic systems (AlCl$_3$ H$_2$SO$_4$)* |
| **MDB conv 40% mono and dialkylated products** |
| EDB and DEB highly reactive conv 70-80% |

## Geometry optimization of molecular structures

The results indicate that the two disubstituted species with fused ring show different lowest-energy forms, twisted in the case of EDB (Figure 1a) and puckered for MDB (Figure 1b). When considering the molecule with free substituents DEB, according to the calculations of Dorofeeva *et al.*[45], it has three stable conformers: anti-anti with a plane backbone, anti-gauche with one orthogonal and gauche-gauche with two orthogonal methyl groups. The absolute minimum corresponds to the anti-anti conformer (Figure 1c), but it is lower than the anti-gauche by less than 1 kcal/mol, while the gauche-gauche is much higher in energy. However, only the planar structure was used for IR assignment and frequencies are reported only for this conformer.



a)                          b)                          c)
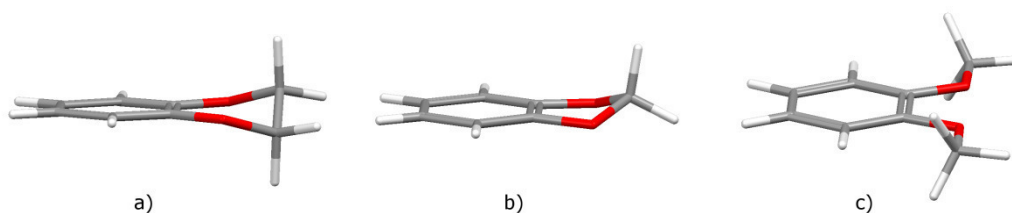
Figure 1. Lowest energy structures for a) EDB, b) MDB, and c) DEB.

These results strongly support the idea that the three molecules should yield different energetically most favored adsorption configurations on the catalyst surface, resulting in a different activation of the benzene ring. Vibrational spectroscopic techniques should be suitable for studying the interaction of the molecules with the catalytic sites. In order to explain the reactivity differences observed in the catalytic tests a FT-IR study of the adsorption of each of the substrates on beta zeolite has been carried out and a comparative analysis using

MDB and EDB was performed on gamma alumina, to be sure that the results are not due to the specific texture of the materials.

## Vibrational assignments

The tables below summarized the vibrational frequencies, experimental and calculated, of free pure molecules. Moreover in the same tables are listed the frequencies related to the adsorption (I, II) on zeolite at increasing amount of aromatic substrates and those related to the desorption step at increasing temperature (room temperature, 100°C, 200°C, and 500°C).

Vibrational assignments of experimental infrared spectra have been made by comparing them with those previously reported in literature[46–49] and with the computed ones. The frequencies and the intensities of the experimental infrared spectra of the three molecules are quite nicely predicted by the calculation, and almost all the computed frequencies are easily assigned to observed bands even if in some cases this requires several reassignments compared the literature.[46–49]

## HBEA and γ-Al$_2$O$_3$ FT-IR characterization

The spectrum of calcined zeolite after evacuation at 500 °C shows four signals at 3779, 3742, 3660 and 3604 cm$^{-1}$ (Figure 2, solid line). The two main peaks at 3742 and 3604 cm$^{-1}$ correspond to terminal silanols and bridging framework Si−OH−Al groups, respectively. The other two small peaks at 3779 and 3660 cm$^{-1}$ have been attributed respectively both to the Al−OH species, being near to Si−OH groups generated when Al leaves the framework, and to the hydroxyls associated with extra-framework aluminum.[25–27] The four OH peaks are superimposed on a broad band at 3700-3200 cm$^{-1}$ due to the hydrogen-bonded bridging OH groups.[26]
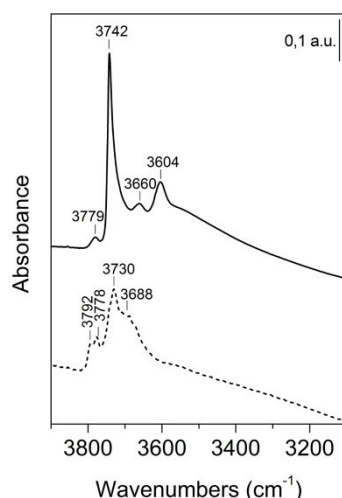


Figure 2. FTIR spectra (hydroxyl vibration region) of HBEA (solid spectrum) and γ-Al$_2$O$_3$ (dashed spectrum) samples after evacuation at 500 °C for 6 hours.

The alumina spectrum after evacuation at 500 °C (Figure 2, dashed line) shows the typical signals attributed to the different types of hydroxyl groups. In particular the main bands at 3792/3778, 3730 and 3688 cm$^{-1}$ may be attributed to isolated hydroxyl groups of I, II and III type, while the broad band centered around 3580 cm$^{-1}$ is due to the H-bonded hydroxyl groups. [50–54]

## Interaction of MDB with HBEA and γ-Al$_2$O$_3$

The formation of a hydrogen-bonded adduct is evident after adsorption of MDB, as confirmed by the strong spectral perturbations shown in Figure 3, whereas all vibrational assignments are summarized in Table 3.

Table 3. Vibrational assignments (cm$^{-1}$) for MDB

| | Description | Wavenumbers (cm$^{-1}$) | | | | | | |
|---|---|---|---|---|---|---|---|---|
| | | Pure calculated[a] | Pure | Adsorptions | | Desorptions | | |
| | | | | I | II | 100°C | 200°C | 500°C |
| Zeolite | ν Al−OH near SiOH | | 3779 | | | | | |
| | ν Si−OH terminal | | 3742 | 3743 | 3742 | 3745 | 3744 | 3745 |
| | ν Al−OH extra-framework Al | | 3660 | | | | | |
| | ν Si−OH−Al bridging framework | | 3604 | | | | | |
| | | | | | | | | |
| MDB | H-bondend complex | | | 3530 | 3511 | 3542 | 3543 | |
| | ν sym ip C−H | 3082 | 3097 | 3097 | 3097 | | | |
| | ν asym ip C−H | 3078 | 3066 | 3068 | 3068 | 3068 | 3065 | 3064 |
| | ν sym op C−H | 3066 | 3050 | 3036 | 3035 | 3035 | | |
| | ν asym op C−H | 3053 | 3011 | | | | | |
| | ν asym op CH$_2$ | 3046 | 2981 | 2982 | 2992 | 2992 | | |
| | ν CH$_2$ (CH···OSi) | | | 2916 | 2916 | 2919 | 2926 | |
| | ν sym C−H (CH$_2$) | 2896 | 2891 | 2891 | 2891 | | | |
| | ν C−C Benzene | 1589 | 1628 | | | | | |
| | ν C−C Benzene | 1577 | 1604 | 1606 | 1606 | 1605 | 1600 | 1602 |
| | δ$_s$ CH$_2$ | 1487 | 1501 | 1502 | 1502 | 1504 | | |
| | ν C−C Benzene + ν sym CCO | 1445 | 1479 | 1478 | 1477 | | | |
| | ν C−C Benzene + ν asym CCO | 1420 | 1447 | 1444 | 1445 | 1445 | | |
| | ν C−C Benzene | 1398 | 1361 | 1361 | 1361 | | | |
| | ν sym C−C−O | 1237 | 1232 | 1237 | 1237 | | | |
| | ω op, op' C−H | 1114 | 1152 | | | | | |
| | ν C−C Benzene + ν asym CO | 1112 | 1125 | | | | | |
| | ν C−C Benzene + ν asym CO | 1054 | 1092 | | | | | |
| | ν sym O−C−O | 1027 | 1041 | 1051 | | | | |

Abbreviations: ν, stretching; ω, wagging; τ, twisting; δs, scissoring; ρ, rockin; ip, in phase; op, out of phase.

[a] Calculated at MP2(FC) level using the 6311G(d,p) basis set by the Gaussian09 software package.[41] IR frequencies were scaled by a factor of 0.9496.[42]

[b] Pure gas phase molecule.

On increasing the dosage of MDB, the band at 3742 cm$^{-1}$ is strongly eroded and the other hydroxyl bands (3779, 3660 and 3604 cm$^{-1}$) disappear completely. Simultaneously, an intense band centered at 3530 cm$^{-1}$ grows and shifts toward lower wavenumbers (3513 cm$^{-1}$) with increasing MDB coverage, as shown in Figure 3.
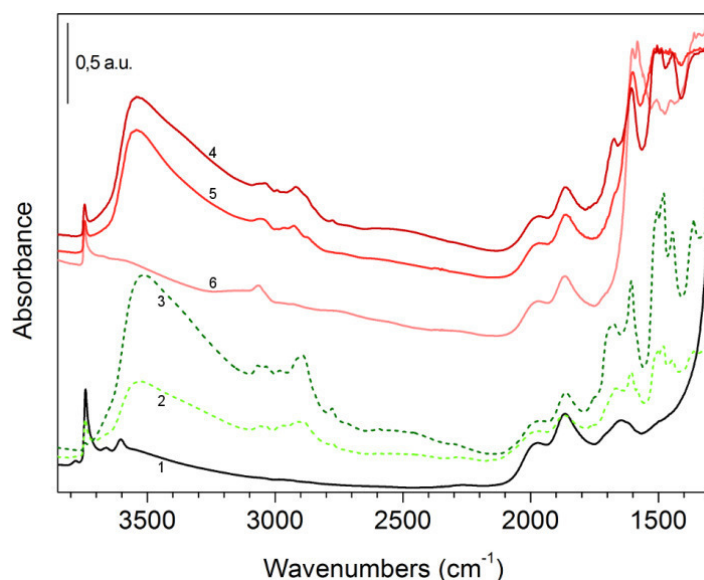


Figure 3. FTIR spectra of HBEA with increasing amount of MDB, followed by evacuation at increasing temperatures. (1) solid black spectrum, HBEA calcined at 500°C for 6 hours; dashed green scale spectra, adsorption of MDB at RT (2) medium and (3) high coverages; solid red scale spectra, desorption steps at increasing temperature (4) 100°C, (5) 200°C and (6) 500°C.



a)                                       b)
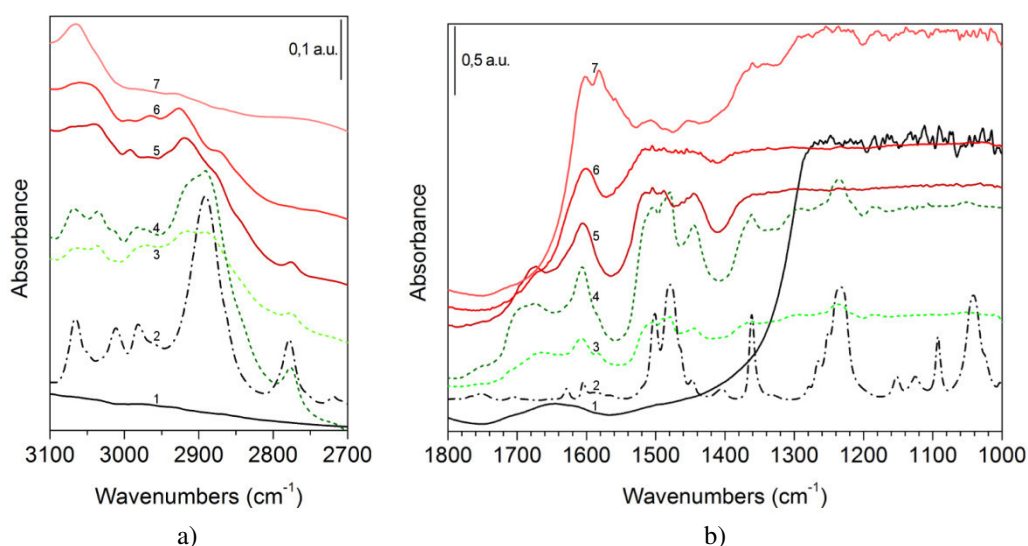
Figure 4. FTIR spectra, (a) in the C−H stretching region and (b) in the region 1800−1000 cm$^{-1}$, of increasing dosages of MDB on HBEA followed by evacuation at increasing temperature. (1) solid black spectrum, HBEA calcined at 500°C for 6 hours; (2) dashed-dotted black spectrum, pure MDB; dashed green scale spectra, adsorption of MDB at RT (3) medium and (4) high coverages; solid red scale spectra, desorption steps at increasing temperature (5) 100°C, (6) 200°C and (7) 500°C.

The present results show that all hydroxyl groups are strongly affected by the adsorption of MDB; this strong interaction is confirmed by the presence of a very intense and irreversible[28,55,56] adsorption (the zeolite feature is not totally restored after outgassing at 500°C) due to the formation of an H-bonded complex. Considering the strength of the linkage, it is possible to hypothesize the formation of a strong H-bond between the zeolite and the organic substrate ($_{zeolite}O-H\cdots O_{MDB}$) due to a preferential adsorption through oxygen atoms.[27,57–60] The changes in relative intensity of some band after heating at high temperature may be ascribed to the partial decomposition of the molecule. Two broad bands near 3090 and 2450 cm$^{-1}$ with a window in the middle, near 2700 cm$^{-1}$ may be associated with Fermi resonance produced by interactions of the acidic zeolite OHs with a base, in this case MDB (Figure 3).[27,55,58,61]

It is difficult to interpret the spectra in the (aliphatic and aromatic) C−H stretching region, shown in Figure 4a, as the differences in the vibrational properties, caused by interaction with the zeolite, are rather complex. With regard to the aromatic ring the most evident spectral perturbation is the shift of the band at 3050 cm$^{-1}$ toward lower wavenumbers, probably due to the strong H-bond between oxygen and silanols that perturbs the electronic cloud of the aromatic ring. The appearance, in the CH$_2$ stretching region, of a new band at 2916 cm$^{-1}$ may be ascribed to the interaction between the hydrogens of the methylene group and the oxygen of the zeolite lattice. Consequently, the CH$_2$ deformation at 1501 cm$^{-1}$ is also perturbed, resulting in a shift toward higher wavenumbers (Figure 4b). Focusing the attention on the spectral region between 1800 and 1000 cm$^{-1}$ (Figure 4b), it is possible to see that the bands due to C−C ring vibrations are almost unaffected by adsorption, thus indicating that there is no direct interaction of the aromatic ring with the catalyst. The vibrational modes of C−O are strongly perturbed, in particular the C−C−O symmetric and asymmetric stretching at 1479 and 1447 cm$^{-1}$ are shifted toward lower wavenumbers, while the C−C−O symmetric stretching at 1232 cm$^{-1}$ and O−C−O asymmetric stretching at 1041 cm$^{-1}$ are shifted toward higher wavenumbers. These latter results confirm that interaction occurs preferentially through oxygen atoms; the MDB maintains the puckered conformation after adsorption, resulting in an electronic deactivation of benzene ring[62] and forcing the benzene ring to stay far from catalyst surface.

A similar behavior has been observed in the case of alumina (Figure 5). Adsorption of MDB strongly perturbs the hydroxyl groups of alumina, resulting in the growth of the strong band centered around 3540 cm$^{-1}$. Changes observed in C−C and C−H stretching vibrations follow the same behavior which has been already observed for zeolite. As in case of zeolite a negligible shift of the C−C and C−H stretching of benzene ring is observed, while strong changes in C−O and CH$_2$ vibrational modes occur. In particular, aliphatic C−H stretching at 2891 cm$^{-1}$ shifts to lower wavenumbers, while the bands attributed to C−C−O vibrations (1479, 1447 and 1232 cm$^{-1}$) and the one associated to symmetric O−C−O stretching at 1041 cm$^{-1}$ are

shifted to higer wavenubers. News bands at 1598 and 1497 cm$^{-1}$ and in the region between 1330-1220 cm$^{-1}$, still detectable after evacuation at 500°C, may be assigned to the formation of phenate species due to the partial decomposition of MDB.[63]
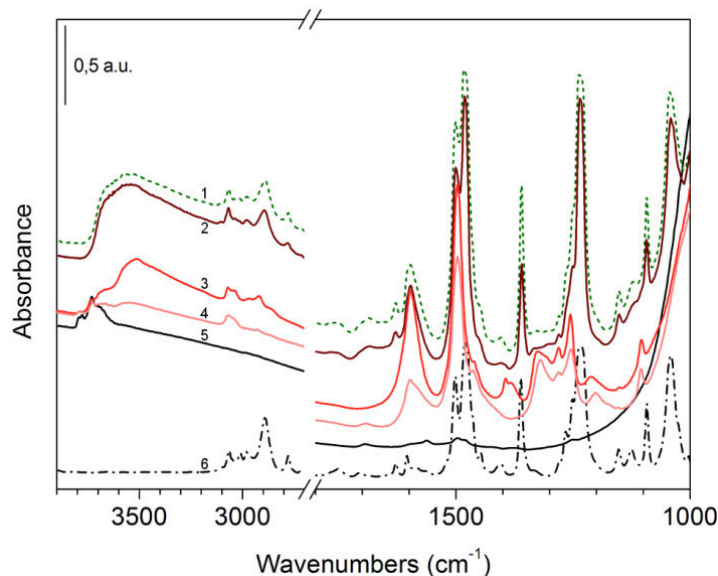


Figure 5. Changes in FTIR spectra of γ-Al$_2$O$_3$ produced by adsorption of MDB followed by desorption at increasing temperature. (1) Green dashed spectrum, adsorbed MDB; solid red scale spectra, desorption steps at increasing temperature (2) RT, (3) 200°C and (4) 500°C; (5) solid black spectrum, γ-Al$_2$O$_3$ after evacuation at 500°C for 6 hours; (6) dashed-dotted black black spectrum, pure MDB.

## Interaction of EDB with HBEA and γ-Al$_2$O$_3$

A detailed analysis of FT-IR spectra of adsorbed EDB on zeolite sample is reported below, whereas the vibrational frequencies are reported in Table 4.

As shown in Figure 6, upon increasing the EDB load the silanol band at 3783 cm$^{-1}$ gradually disappears, with a parallel growth of a small adsorption at 3686 cm$^{-1}$, which may be attributed to the interaction of the aromatic ring with silanol groups.[25,26] The remaining silanol bands (3746, 3667 and 3610 cm$^{-1}$) are almost unaffected, whereas the broad band at 3700-3200 cm$^{-1}$ results in an increase in intensity and in a shift toward lower wavenumbers. A shoulder at about 3250 cm$^{-1}$ may be attributed to the H-bonding complex of the benzene ring and bridging OHs according to Trombetta et al.[33] Upon formation of a weak hydrogen bond, in Figure 6 it is possible to distinguish two broad bands in the region of 2970 and 2420 cm$^{-1}$ with a window at around 2600 cm$^{-1}$ attributable to the A and B components of Fermi resonance.[27,55,58,61]

Table 4. Vibrational assignments (cm$^{-1}$) for EDB.

| | Description | Wavenumbers (cm$^{-1}$) | | | | | | | | |
|---|---|---|---|---|---|---|---|---|---|---|
| | | Pure calculated[a] | Pure | Adsorptions | | | Desorptions | | | |
| | | | | I | II | III | RT | 100°C | 200°C | 500°C |
| Zeolite | ν Al–OH near SiOH | | 3783 | 3783 | | | | | | 3778 |
| | ν Si–OH terminal | 3746 | 3746 | 3746 | 3746 | 3746 | 3745 | 3744 | 3744 | 3742 |
| | ν Al–OH extra-framework Al | 3667 | 3668 | 3668 | 3668 | | | | 3663 | 3661 |
| | ν Si–OH–Al bridging framework | 3610 | 3610 | 3607 | | | | | 3608 | 3603 |
| | | | | | | | | | | |
| EDB | H-bondend silanols | | | | 3535 | 3459 | 3487 | 3531 | | |
| | ν sym ip C–H | 3075 | 3091 | | | | | | | |
| | ν asym ip C–H | 3066 | 3076 | | 3078 | 3078 | 3078 | 3078 | | |
| | ν sym op C–H | 3059 | 3062 | | | 3065 | 3066 | | | |
| | ν asym op C–H | 3049 | 3043 | | 3047 | 3047 | 3047 | 3048 | | |
| | ν asym op CH$_2$ | 3012 | 2980 | 2984 | 2980 | 2980 | 2981 | 2984 | | |
| | ν asym ip CH$_2$ | 3010 | 2934 | 2940 | 2936 | 2936 | 2937 | 2941 | | |
| | ν sym ip CH$_2$ | 3923 | 2879 | 2886 | 2883 | 2883 | 2884 | 2887 | | |
| | Polydentate | | | | 1708 | 1708 | 1708 | 1704 | | |
| | Polydentate | | | 1676 | 1693 | 1693 | 1691 | 1690 | 1675 | |
| | ν C–C Benzene + ν asym CCO | 1574 | 1605 | | 1608 | 1608 | 1608 | 1609 | | |
| | ν C–C Benzene | 1552 | 1594 | | 1596 | 1596 | 1596 | 1598 | 1592 | |
| | ν C–C Benzene + ν sym CCO | 1459 | 1495 | 1496 | 1496 | 1496 | 1496 | 1496 | 1496 | |
| | δ$_s$ ip CH$_2$ | 1435 | 1467 | 1467 | 1467 | 1467 | 1467 | 1468 | 1468 | |
| | ω ip C–H | 1413 | 1453 | 1453 | 1454 | 1454 | 1454 | 1454 | | |
| | Polydentate | | | | 1419 | 1419 | 1419 | 1415 | | |
| | ν C–C Benzene | 1394 | 1381 | | | | | | | |
| | Polydentate | | | 1370 | 1370 | 1371 | 1370 | 1364 | 1362 | |
| | ω op CH$_2$ | 1359 | 1309 | | 1308 | 1308 | 1308 | 1307 | | |
| | τ ip CH$_2$ | 1263 | 1279 | | | | | | | |
| | ν sym C–O–C | 1234 | 1251 | | | | | | | |
| | ν asym C–O–C | 1162 | 1194 | | | | | | | |
| | ω op, op' C–H | 1112 | 1150 | | | | | | | |
| | ω ip, op' C–H | 1080 | 1112 | | | | | | | |

Abbreviations: ν, stretching; ω, wagging; τ, twisting; δs, scissoring; ρ, rockin; ip, in phase; op, out of phase.

[a] Calculated at MP2(FC) level using the 6311G(d,p) basis set by the Gaussian09 software package.[41] IR frequencies were scaled by a factor of 0.9496.[42]

[b] Pure gas phase molecule.

On the basis of these results, it is possible to hypothesize the planar adsorption of EDB on the catalyst surface, considering that: i) there is no evidence of interaction between the oxygen atoms of EDB and silanols ii) the perturbation of H-bonded hydroxyls is caused by delocalized π-type orbitals of aromatics.[31] The interaction is completely reversible and by far weaker than that observed in the case of MDB, as confirmed by the total restoration of the original spectrum when the temperature reaches at 200°C.
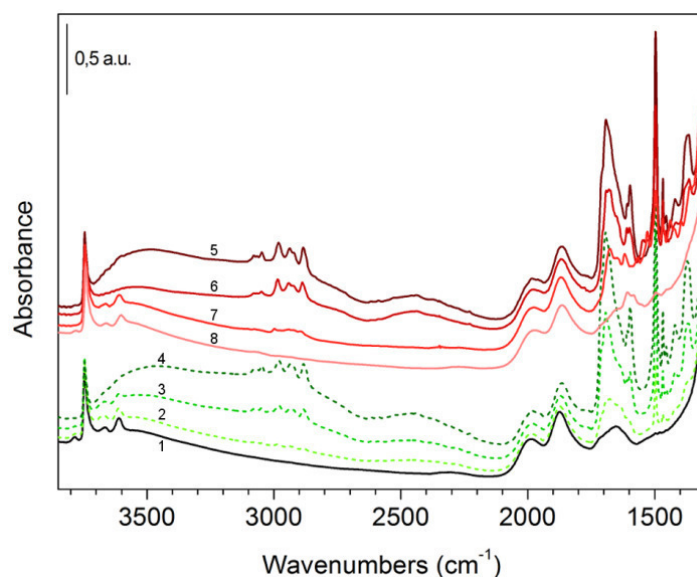
Figure 6. FTIR spectra of HBEA with increasing amount of EDB, followed by evacuation at increasing temperatures. (1) solid black spectrum, HBEA calcined at 500°C for 6 hours; dashed green scale spectra, adsorption of EDB at RT (2) low, (3) medium and (4) high coverages; solid red scale spectra, desorption steps at increasing temperature (5) RT, (6) 100°C, (7) 200°C and (8) 500°C.

Our previous hypothesis is supported by the shift upward of all the aromatic CH and aliphatic $CH_2$ stretching vibrations; a shift which increases with temperature, thus indicating the formation of stronger bonded species (see Figure 7a).



a)                                                b)
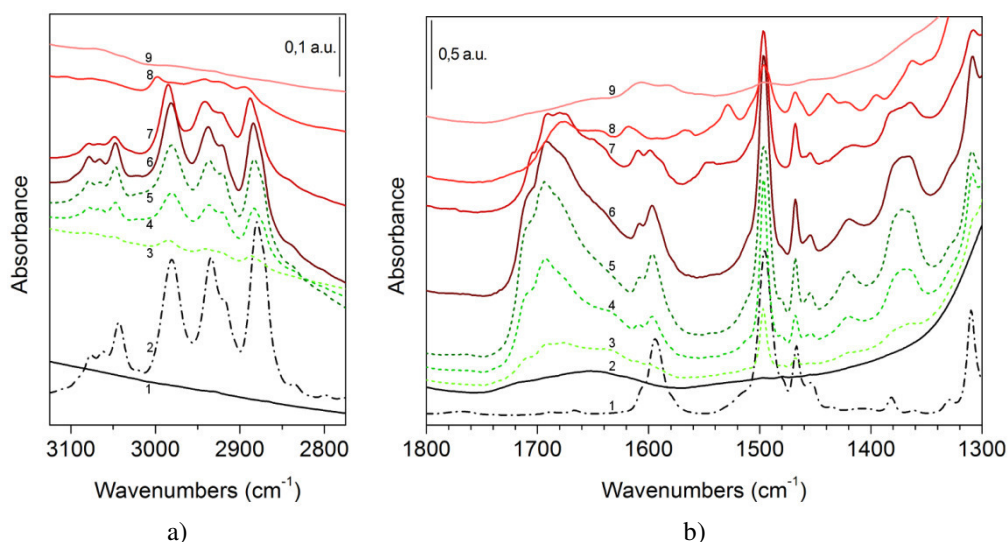
Figure 7. FTIR spectra, (a) in the C−H stretching region and (b) in the region 1800−1300 cm$^{-1}$, of increasing dosages of EDB on HBEA followed by evacuation at increasing temperature. (1) Solid black spectrum, HBEA calcined at 500°C for 6 hours; (2) dashed-dotted black spectrum, pure EDB; dashed green scale spectra, adsorption of EDB at RT (3) low, (4) medium and (5) high coverages; solid red scale spectra, desorption steps at increasing temperature (6) RT, (7) 100°C, (8) 200°C and (9) 500°C.

Moreover, analyzing the region between 1800 and 1300 cm$^{-1}$ (Figure 7b), the shift upward of C−C stretching vibrations is a further evidence that EDB adsorption

occurs through the benzene ring, then the interaction involves C=C π-type orbitals, as reported by Trombetta et al.[31,33] In the same region an intense band at 1693 cm$^{-1}$, with a shoulder at 1708 cm$^{-1}$, and two bands at 1419 cm$^{-1}$ and 1370 cm$^{-1}$ appear. These three latter bands are due to the formation of a bicoordinated adduct in which one of the two methylene carbons interacts with two adjacent oxygens of the zeolite lattice. This interaction may be ascribed to the complex formed by $CO_2$ with zeolite oxygen, such as observed by Lavalley[64] and Wirawan *et al.*[65] These last results confirm that EDB interacts predominately through the benzene ring and methylene group instead of oxygen, maintaining a planar conformation.

The adsorption of EDB on alumina (Figure 8) confirm the hypothesis of its planar adsorption. In particular the appearance of the bands at 1701, 1690, 1423 and 1368 cm$^{-1}$ confirm the formation of the bicoordinated adduct. Also in this case phenate species strongly adsorbed on alumina are formed, such as confirmed by the presence of bands at 1592, 1496 cm$^{-1}$ and in the region 1320-1220 cm$^{-1}$.[63]
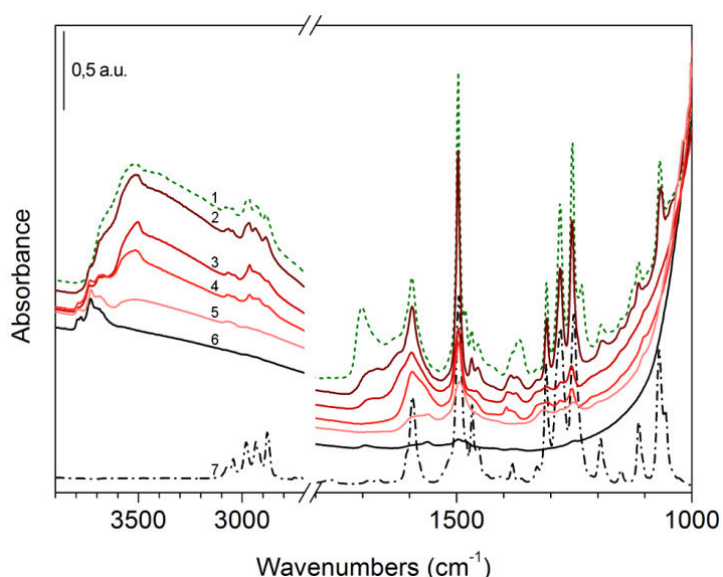


Figure 8. Changes in FTIR spectra of γ-Al$_2$O$_3$ produced by adsorption of EDB followed by desorption at increasing temperature. (1) green dashed spectrum, adsorbed EDB; solid red scale spectra, desorption steps at increasing temperature (2) RT, (3) 100°C, (4) 200°C and (5) 500°C; (6) solid black spectrum, γ-Al2O3 after evacuation at 500°C for 6 hours; (7) dashed-dotted black black spectrum, pure EDB.

## Interaction of DEB with HBEA

DEB shows both kinds of interaction already observed separately for EDB and MDB; Table 5 summarizes these results.

Table 5. Vibrational assignments (cm$^{-1}$) for DEB.

| | Description | Wavenumbers (cm$^{-1}$) | | | | | | | |
|---|---|---|---|---|---|---|---|---|---|
| | | Pure calculated[a] | Pure | Adsorptions | | Desorptions | | | |
| | | | | I | II | RT | 100°C | 200°C | 500°C |
| Zeolite | ν Al−OH near SiOH | | 3779 | | | | | | 3778 |
| | ν Si−OH terminal | | 3741 | 3745 | | | 3744 | 3743 | 3741 |
| | ν Al−OH extraframework Al | | 3661 | | | | | | 3662 |
| | ν Si−OH−Al bridging framework | | 3603 | | | | | | 3601 |
| DEB | H-bondend silanols | | | 3588 | 3584 | 3592 | 3598 | | |
| | H-bonded complex | | | 3469 | 3462 | 3464 | 3493 | 3532 | |
| | ν sym ip C−H | 3087 | 3107 | 3109 | 3011 | 3113 | 3113 | | |
| | ν sym ip C−H | 3084 | 3078 | | | | | | |
| | ν asym op C−H | 3065 | 3064 | 3070 | 3068 | 3069 | 3073 | 3072 | 3065 |
| | ν sym op C−H | 3049 | 3045 | 3047 | 3048 | 3049 | 3049 | | |
| | ν asym ip CH$_3$ | 3039 | 3000 | 3004 | 3002 | 3002 | 3007 | 3005 | |
| | ν asym op CH$_3$ (CH···OSi) | 2971 | 2954 | 2967 | 2967 | 2967 | 2968 | 2963 | |
| | ν CH$_3$ | | 2944 | 2947 | 2947 | 2949 | 2952 | | |
| | ν CH$_3$ | | 2934 | 2936 | | | | | |
| | ν CH$_3$ | | 2906 | 2912 | 2912 | 2912 | 2918 | | |
| | ν CH$_3$ | | 2889 | 2892 | 2892 | 2893 | 2898 | | |
| | ν sym op CH$_3$ | 2898 | 2835 | 2842 | 2840 | 2840 | 2846 | | |
| | Polydentate | | | 1710 | 1710 | 1710 | 1710 | | |
| | Polydentate | | | 1694 | 1694 | 1694 | 1673 | 1670 | |
| | ν C−C Benzene + ν asym CCO | 1563 | 1592 | 1596 | 1595 | 1595 | 1599 | 1599 | 1598 |
| | ν C−C Benzene + ν asym CCO | 1480 | 1506 | 1505 | 1500 | 1500 | 1504 | 1504 | |
| | δ$_s$ HCH (CH3) | 1457 | 1463 | 1466 | 1465 | 1465 | 1468 | 1468 | |
| | δ$_s$ HCH (CH3) | 1435 | 1442 | 1444 | 1444 | 1444 | 1446 | | |
| | Polydentate | | | 1420 | 1420 | | | | |
| | Polydentate | | | 1368 | 1364 | 1363 | | | |
| | δ$_{umbrella}$ CH$_3$ | 1421 | 1330 | | 1327 | 1326 | | | |
| | δ$_{umbrella}$ CH$_3$ | 1399 | 1286 | | | | | | |
| | ν$_{sym}$PhO + ν C−C + CH in plane bend | 1255 | 1254 | | | | | | |
| | ν$_{asym}$PhO + ν C−C + CH in plane bend | 1211 | 1230 | | | | | | |
| | ρ CH$_3$ | 1157 | 1176 | | | | | | |
| | CH in plane bending | 1096 | 1123 | | | | | | |
| | ν sym O−CH$_3$ | 1042 | 1052 | | | | | | |
| | ν sym O−CH$_3$ | 1019 | 1028 | | | | | | |

Abbreviations: ν, stretching; ω, wagging; τ, twisting; δs, scissoring; ρ, rockin; ip, in phase; op, out of phase.

[a] Calculated at MP2(FC) level using the 6311G(d,p) basis set by the Gaussian09 software package.[41] IR frequencies were scaled by a factor of 0.9496.[42]

[b] Pure gas phase molecule.

In particular, as observed for MDB, the formation of a strong H-bond between ether groups and zeolite hydroxyls leads to the erosion of the two bands at 3779 and 3741 cm$^{-1}$ and the simultaneous formation of a broad band centered at 3469 cm$^{-1}$.[27,57–60]

The shoulder at 3588 cm$^{-1}$ is ascribable to the perturbation of H-bonded silanols caused by interaction with the benzene ring, as previously evidenced for EDB (Figure 9).[25,26] The absence of an additional fused ring, which forces the molecule to stay in a preferential conformation, leads DEB to interact simultaneously by the oxygen atoms and the benzene ring. Also in this case the two components of Fermi resonance (A and B) may be observed respectively at 2960 and 3440 cm$^{-1}$ (Figure 9).[27,55,58,61]
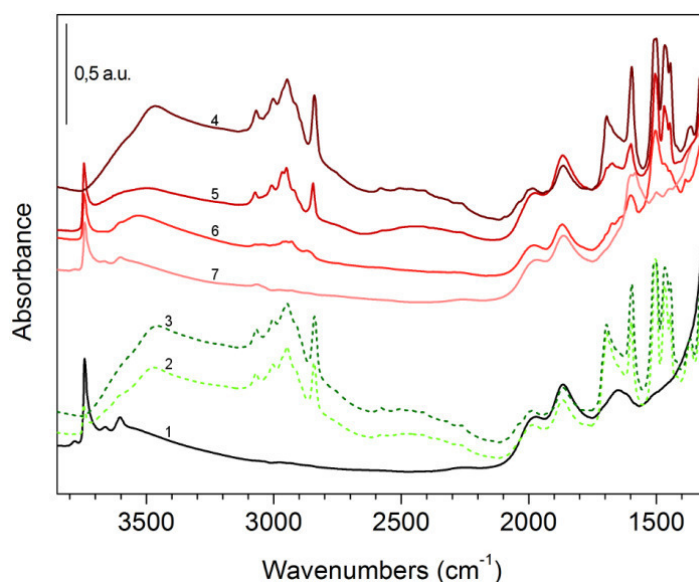


Figure 9. FTIR spectra of increasing dosages of DEB on HBEA followed by evacuation at increasing temperature. (1) solid black spectrum, H-BEA calcined at 500°C for 6 hours; dashed green scale spectra, adsorption of DEB at RT (2) medium and (3) high coverages; solid red scale spectra, desorption steps at increasing temperature (4) RT, (5) 100°C, (6) 200°C and (7) 500°C.



a)                                                          b)
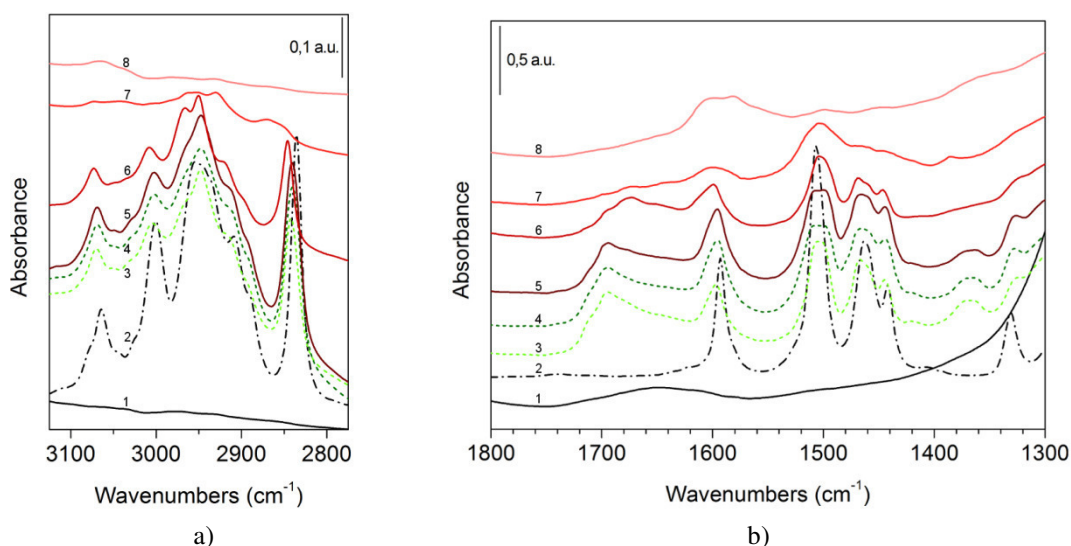
Figure 10. FTIR spectra, a) in the C−H stretching region and b) in the region 1800−1300 cm$^{-1}$, of increasing dosages of DEB on H-BEA followed by evacuation at increasing temperature. (1) solid black spectrum, H-BEA calcined at 500°C for 6 hours; (2) dashed-dotted black spectrum, pure DEB; dashed green scale spectra, adsorption of DEB at RT (3) medium and (4) high coverages; solid red scale spectra, desorption steps at increasing temperature (5) RT, (6) 100°C, (7) 200°C and (8) 500°C.

As shown in Figure 10b, peaks attributed to aromatic moiety are shifted slightly upward, such as in the case of EDB, suggesting that a planar adsorption of the benzene ring occurs on zeolite, as confirmed by benzene C−C stretchings at 1506 and 1592 cm$^{-1}$, also perturbed (Figure 10b).

Aliphatic C−H stretching bands are shifted to higher frequencies and, as in the adsorption of MDB, a splitting of the component at 2954 cm$^{-1}$ is observed (Figure 10a). This latter result may be attributed to the interaction between the hydrogens of the methyl groups and the oxygens of the zeolite framework. Therefore, the $CH_3$ deformation bands at 1463 and 1442 cm$^{-1}$ also result in a shift to higher wavenumbers. The only partial disappearance of DEB signals, even after desorption at 500°C, indicates its strong interaction with the zeolite, as in case of MDB.[28,55,56] As expected from previous considerations on EDB, the bands at 1694 cm$^{-1}$ (shoulder at 1710 cm$^{-1}$), 1420 and 1368 cm$^{-1}$ grow due to the formation of polydentate species[64,65] due to the interaction between $CH_3$ and zeolite oxygen.

Comparing the data obtained in the catalytic tests with the spectroscopic data it is possible to propose different modes of adsorption of the aromatic substrates on considered materials. In the case of MDB the FT-IR findings show that the interaction occurs almost exclusively between hydroxyl groups of the catalyst and oxygen atoms of the substrate, thus the adsorbed MDB molecule maintains the puckered conformation leading the benzene ring far from catalyst surface, as shown in Figure 11 for zeolite. Figure 12 shows the hypothesized model for the adsorption of EDB on zeolite, for which the twisted geometry of the molecule is suitable for a planar linkage through benzene ring and the methylene group without involving the oxygen atom.
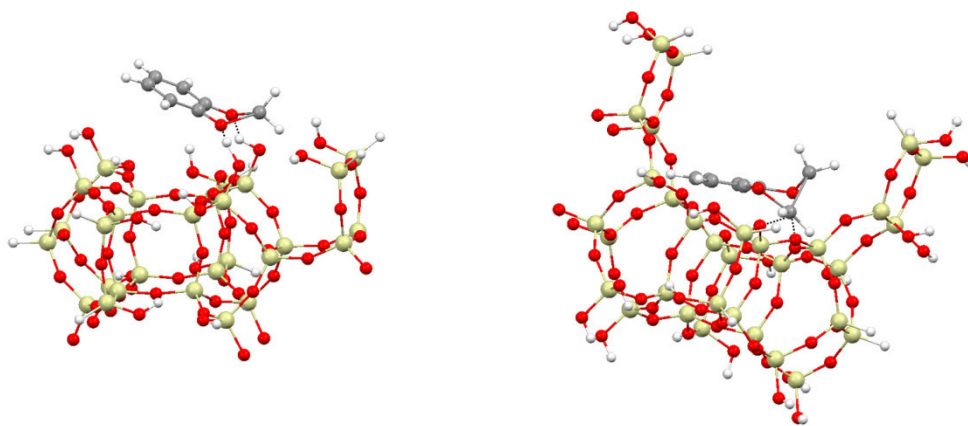


Figure 11. Proposed model for MDB adsorption on H-BEA.

Figure 12. Proposed model for EDB adsorption on H-BEA.

Also, in this case, the configuration of the free molecule is maintained after adsorption. The conformational mobility of free methoxy groups allows DEB molecule to maintain a planar geometry during the adsorption, with simultaneous

interaction through oxygen atoms and benzene ring, as demonstrated by FT-IR analysis.

The above results may be useful in clarifying the different reactivity previously observed in the catalytic tests. All three investigates substrates were reactive in homogenous conditions, in which geometrical conformational changes may occur. On the contrary, the same behavior is not possible using heterogeneous catalysts, on which the molecules are forced to maintain a specific conformation.

The planar orientation in case of EDB and DEB allows the aromatic ring to stay close to catalyst surface, then the molecules may react quickly with activated alkylating agents. Conversely, in the case of MDB the molecule remains in the puckered conformation thus the aromatic ring is almost orthogonal to catalyst surface and electron-deficient, then deactivated, because the oxygen p-orbital can interact predominantly with the methylene group orbital as reported by Moon.[62] These effects deactivate the benzene ring resulting in a complete chemical inertia of MDB on tested catalysts.

# CONCLUSIONS

The nature of the interaction on two different catalysts (zeolite BEA and γ-alumina) of some methoxy substituted benzenes, 1,2-methylendioxybenzene (MDB), 1,2-ethylendioxybenzene (EDB), 1,2-dimethoxybenzene (DEB), have been investigated by FT-IR spectroscopy supported by computational geometry investigation. Overall results demonstrate that the molecular conformation plays a fundamental role in the reactivity of benzene derivatives in alkylation reactions carried out on heterogeneous catalysts. The ab initio calculation showed that the three aromatic substrates have different lowest-energy conformations, in particular puckered for MDB, twisted for EDB and anti-anti for DEB. These results were experimentally confirmed by FT-IR spectroscopy; in fact, the calculated frequencies are in agreement with the experimental ones. In the case of DEB the calculated bands are quite different from the experimental ones because the simulation has been done only for the lowest energy conformer. The deep FT-IR investigation of the adsorption and desorption behavior of the considered substrates allowed to demonstrated that adsorbed molecules maintained the geometry of the free ones.

The twisted conformation of EDB and the absence of a fused ring in case of DEB cause an orientation of the molecules parallel to the catalyst surface, with the benzene ring directly bonded to it and suited for electrophilic attack. MDB adsorption through oxygen atoms holds the molecule in the puckered conformation, maintaining the benzene ring far from the catalyst surface and electron-deficient, then deactivated towards electrophilic alkylation. Finally, the reactivity of MDB in homogeneous catalytic systems, observed in the tests performed in presence of $AlCl_3$ and $H_2SO_4$ may be explained by the conformational changes which are possible in these conditions, whereas not in a heterogeneous one. Difference in

reactivity observed for the three aromatic substrates can definitively be attributed to the geometrical conformation of molecule which induced a different interaction of benzene moiety with catalyst surface.

# REFERENCES

(1)     Lucarelli, C.; Giugni, A.; Moroso, G.; Vaccari, A. *J. Phys. Chem. C* **2012**, *116*, 21308-21317.

(2)     Patinkin, S. H.; Friedman, B. S. In *Friedel-Crafts and Related Reactions*; George A. Olah, 1964; Vol. 2.

(3)     Hoelderich, W. F. *Catal. Today* **2000**, *62*, 115-130.

(4)     Tanabe, K.; Hölderich, W. F. *Appl. Catal., A* **1999**, *181*, 399-434.

(5)     Degnan, Thomas F., J.; Smith, C. M.; Venkat, C. R. *Appl. Catal., A* **2001**, *221*, 283-294.

(6)     Siffert, S.; Gaillard, L.; Su, B.-L. *J. Mol. Catal. A: Chem.* **2000**, *153*, 267-279.

(7)     Perego, C.; Ingallina, P. *Catal. Today* **2002**, *73*, 3-22.

(8)     Čejka, J.; Wichterlová, B.; Bednářová, S. *Appl. Catal., A* **1991**, *79*, 215-226.

(9)     Brechtelsbauer, C.; Emig, G. *Appl. Catal., A* **1997**, *161*, 79-92.

(10)     Ahedi, R. K.; Tawada, S.; Kubota, Y.; Sugi, Y.; Kim, J. H. *J. Mol. Catal. A: Chem.* **2003**, *197*, 133-146.

(11)     Sugi, Y.; Kubota, Y.; Hanaoka, T.-aki; Matsuzaki, T. *Catal. Surv. Jpn.* **2001**, *5*, 43-56.

(12)     Bejblová, M.; Žilková, N.; Čejka, J. *Res. Chem. Intermed.* **2008**, *34*, 439-454.

(13)     Giugni, A.; Impalà, D.; Piccolo, O.; Vaccari, A.; Corma, A. *Appl. Catal., B* **2010**, *98*, 72-78.

(14)     Vanelle, P.; Meuche, J.; Maldonado, J.; Crozet, M. P.; Delmas, F.; Timon-David, P. *Eur. J. Med. Chem.* **2000**, *35*, 157-162.

(15)     Borzatta, V.; Capparella, E.; Gobbi, C.; Poluzzi, E. *Process for synthesizing heliotropine and its derivatives,* US Patent 7,402,709 2008.

(16)     Kushiro, M.; Masaoka, T.; Hageshita, S.; Takahashi, Y.; Ide, T.; Sugano, M. *J. Nutr. Biochem.* **2002**, *13*, 289-295.

(17)     Scriabine, I. *Bull. Soc. Chim. Fr.* **1961**, 1197-1198.

(18)     Valentine, R. H.; Brandman, H. A. *Process for the preparation of dihydrocinnamaldehyde derivates,* US Patent 4,389,527, 1983.

(19)     Shirai, M.; Yoshida, Y.; Sadaike, S. *Process for the production of 1-acetoxy-3-(substituted phenyl)propenes,* EP Patent 1,547,509 (A1), 2005.

(20)     Snowden, R.; Birkbeck, A.; Womack, G.; Firmenich SA *Catalytic Scriabine reaction*, US Patent 7,529,983 (B2), 2009.

(21)     Borzatta, V.; Brancaleoni, D. *Process for the synthesis of 5-(α-hydroxyalkyl)benzo[1,3]dioxols*, US Patent 6,342,613, 2000.

(22)    Borzatta, V.; Brancaleoni, D.; Battistini, C. *Process for the synthesis of 5-alkylbenzodioxoles,* EP Patent 1,048,664 (B1) 2000.

(23)    Zelle, R. E.; McClellan, W. J. *Tetrahedron Lett.* **1991**, *32*, 2461-2464.

(24)    Spagnol, M.; Gilbert, L.; Benazzi, E.; Marcilly, C. *Process for the acylation of aromatic ethers*, US Patent 5,817,878 1998.

(25)    Su, B.-L.; Norberg, V. *Zeolites* **1997**, *19*, 65-74.

(26)    Kiricsi, I.; Flego, C.; Pazzuconi, G.; Parker, W.O., J.; Millini, R.; Perego, C.; Bellussi, G. *J. Phys. Chem.* **1994**, *98*, 4627-4634.

(27)    Pazé, C.; Bordiga, S.; Lamberti, C.; Salvalaggio, M.; Zecchina, A.; Bellussi, G. *J. Phys. Chem. B* **1997**, *101*, 4740-4751.

(28)    Bjørgen, M.; Bonino, F.; Kolboe, S.; Lillerud, K.-P.; Zecchina, A.; Bordiga, S. *J. Am. Chem. Soc.* **2003**, *125*, 15863-15868.

(29)    Namuangruk, S.; Pantu, P.; Limtrakul, J. *J. Catal.* **2004**, *225*, 523-530.

(30)    Rungsirisakun, R.; Jansang, B.; Pantu, P.; Limtrakul, J. *J. Mol. Struct.* **2005**, *733*, 239-246.

(31)    Trombetta, M.; Alejandre, A. G.; Solis, J. R.; Busca, G. *Appl. Catal., A* **2000**, *198*, 81-93.

(32)    Raksakoon, C.; Limtrakul, J. *J. Mol. Struct.: THEOCHEM* **2003**, *631*, 147-156.

(33)    Trombetta, M.; Armaroli, T.; Alejandre, A. G.; Solis, J. R.; Busca, G. *Appl. Catal., A* **2000**, *192*, 125-136.

(34)    Ballarini, N.; Cavani, F.; Maselli, L.; Montaletti, A.; Passeri, S.; Scagliarini, D.; Flego, C.; Perego, C. *J. Catal.* **2007**, *251*, 423-436.

(35)    Ballarini, N.; Cavani, F.; Maselli, L.; Passeri, S.; Rovinetti, S. *J. Catal.* **2008**, *256*, 215-225.

(36)    Cavani, F.; Maselli, L.; Passeri, S.; Lercher, J. A. *J. Catal.* **2010**, *269*, 340-350.

(37)    Crocellà, V.; Cerrato, G.; Magnacca, G.; Morterra, C.; Cavani, F.; Maselli, L.; Passeri, S. *Dalton Trans.* **2010**, *39*, 8527-8537.

(38)    Svelle, S.; Bjørgen, M. *J. Phys. Chem. A* **2010**, *114*, 12548-12554.

(39)    Svelle, S.; Visur, M.; Olsbye, U.; Saepurahman; Bjørgen, M. *Top. Catal.* **2011**, *54*, 897-906.

(40)    Bjorgen, M.; Svelle, S.; Joensen, F.; Nerlov, J.; Kolboe, S.; Bonino, F.; Palumbo, L.; Bordiga, S.; Olsbye, U. *J. Catal.* **2007**, *249*, 195-207.

(41)    Frisch, M.; J. Trucks, G. W.; Schlegel, H. B.; Scuseria, G. E.; Robb, M. A.; Cheeseman, J. R.; Scalmani, G.; Barone, V.; Mennucci, B. ; Petersson, G. A.; Nakatsuji, H. et al. *Gaussian 09*, Revision B.01; Gaussian, Inc.: Wallingford, CT, 2010

(42)    Scott, A. P.; Radom, L. *J. Phys. Chem.* **1996**, *100*, 16502-16513.

(43)    Perego, C.; Amarilli, S.; Carati, A.; Flego, C.; Pazzuconi, G.; Rizzo, C.; Bellussi, G. *Microporous Mesoporous Mater.* **1999**, *27*, 345-354.

(44)    Amandi, R.; Licence, P.; Ross, S. K.; Aaltonen, O.; Poliakoff, M. *Org. Process Res. Dev.* **2005**, *9*, 451-456.

(45)    Dorofeeva, O. V.; Shishkov, I. F.; Karasev, N. M.; Vilkov, L. V.; Oberhammer, H. *J. Mol. Struct.* **2009**, *933*, 132-141.

(46)    Emanuele, E.; Negri, F.; Orlandi, G. *Chem. Phys.* **2006**, *321*, 75-85.

(47)    Jeon, S.; Choo, J.; Kim, S.; Kwon, Y.; Kim, J.-Y.; Lee, Y.-I.; Chung, H. *J. Mol. Struct.* **2002**, *609*, 159-167.

(48)    Autrey, D.; Yang, J.; Laane, J. *J. Mol. Struct.* **2003**, *661-662*, 23-32.

(49)    Novikov, V. P.; Yarkov, A. V.; Solotnov, A. F.; Raevskii, O. A. *Russ. Chem. Bull.* **1985**, *34*, 952-958.

(50)    Digne, M.; Sautet, P.; Raybaud, P.; Euzen, P.; Toulhoat, H. *J. Catal.* **2002**, *211*, 1-5.

(51)    Tsyganenko, A. A.; Filimonov, V. N. *J. Mol. Struct.* **1973**, *19*, 579-589.

(52)    Morterra, C.; Magnacca, G. *Catal. Today* **1996**, *27*, 497-532.

(53)    M. Haaland, D. *Surf. Sci.* **1981**, *102*, 405-423.

(54)    Ballinger, T. H.; Yates, J. T. J. *Langmuir* **1997**, 3041-3045.

(55)    Bregolato, M.; Bolis, V.; Busco, C.; Ugliengo, P.; Bordiga, S.; Cavani, F.; Ballarini, N.; Maselli, L.; Passeri, S.; Rossetti, I.; Forni, L. *J. Catal.* **2007**, *245*, 285-300.

(56)    Flego, C.; Kiricsi, I.; Perego, C.; Bellussi, G. *Stud. Surf. Sci. Catal.* **1995**, 405-412.

(57)    Skorpa, R.; Bordiga, S.; Bleken, F.; Olsbye, U.; Arstad, B.; Tolchard, J.; Mathisen, K.; Svelle, S.; Bjørgen, M. *Microporous Mesoporous Mater.* **2011**, *141*, 146-156.

(58)    Zecchina, A.; Spoto, G.; Ricchiardi, G.; Bordiga, S.; Bonino, F.; Prestipino, C.; Lamberti, C. In *Impact of Zeolites and other Porous Materials on the new Technologies at the Beginning of the New Millennium Proceedings of the 2nd International FEZA (Federation of the European Zeolite Associations) Conference*; Aiello, R.; Giordano, G.; Testa, F., Eds.; Elsevier, 2002; Vol. 142, pp. 3-14.

(59)    Bordiga, S.; Regli, L.; Cocina, D.; Lamberti, C.; Bjørgen, M.; Lillerud, K. P. *J. Phys. Chem. B* **2005**, *109*, 2779-2784.

(60)    Barbera, K.; Bonino, F.; Bordiga, S.; Janssens, T. V. W.; Beato, P. *J. Catal.* **2011**, *280*, 196-205.

(61)    Trombetta, M.; Busca, G.; Storaro, L.; Lenarda, M.; Casagrande, M.; Zambon, A. *Phys. Chem. Chem. Phys.* **2000**, *2*, 3529-3537.

(62)    Moon, S.; Kwon, Y.; Lee, J.; Choo, J. *J. Phys. Chem. A* **2001**, *105*, 3221-3225.

(63)    Popov, A.; Kondratieva, E.; Goupil, J. M.; Mariey, L.; Bazin, P.; Gilson, J.-pierre; Travert, A.; Maugé, F. *J. Phys. Chem. C* **2010**, *114*, 15661-15670.

(64)    Lavalley, J. C. *Catal. Today* **1996**, *27*, 377-401.

(65)    Wirawan, S. K.; Creaser, D. *Microporous Mesoporous Mater.* **2006**, *91*, 196-205.

# Chapter 2

# Insights into the reactivity of thiophene: heterogeneous alkylation

## INTRODUCTION

Thiophene derivatives are valuable intermediates in fine chemicals industry, in particular alkyl- and acyl-thiophene compounds are employed as raw materials for the production of biologically active compounds which are widely used in the synthesis of drugs, herbicides/pesticides, aroma and fragrances.[1–3] 2,5-dimethylthiophene (Figure 1a) and 2,5-dimethyl-3-acetylthiophene (Figure 1b) found application in the aroma chemical field, giving the flavor of roasted meats and nutty, respectively. The latter compound has been also employed as precursor for many drugs, for example antibacterial agents (Figure 1f)[4] and anti-inflamatory drugs (Figure 1g)[5]. 2-acetyl-5-methylthiophene (Figure 1c) has been employed as raw material for the synthesis of thiophene ethanolamines[6], which are used as anti-hypertensive drugs. 2-acetylthiophene (Figure 1d) has been employed as precursors of fungicides by Zeneca[7], and as raw material for antidepressant Duloxetine by Eli Lilly.[8] 2-alkylthiophenes (propyl, isopropyl, butyl, pentyl, hexyl, heptyl and octyl), Figure 1e, are precursors of a wide range of products, both in pharmaceutical and fragrances fields: for example 2-octylthiophene has been used in the synthesis of anti-atheroslerotic agent[9] (Figure 1h) and 2-isopropylthiophene is a starting material for Lioral (Figure 1i).[10]
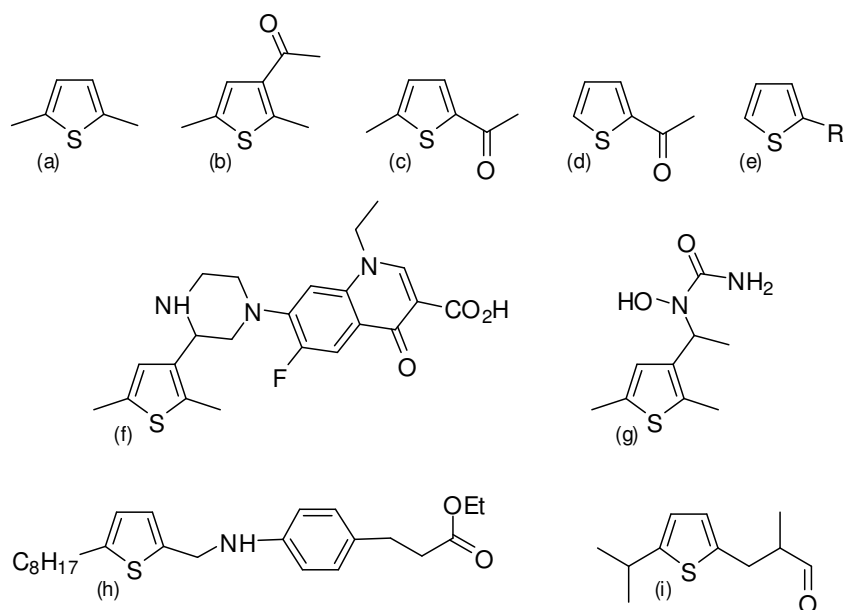
Figure 1. Thiophene derivatives.

## Preparative methods

Synthetic routes for the synthesis of substituted thiophene compounds can be divided in two classes: i) condensation of an appropriately substituted open chain precursors with a suitable sulfurizing agent, ii) direct functionalization of thiophene through electrophilic substitutions.[1–3]

Ciclyzation reactions on industrial scale are performed in vapor phase starting from different carbon skeleton precursors (variously substituted alcohols, aldehydes, ketones or olefins) in presence of $CS_2$ or $H_2S$ and using metal oxides as catalysts, Figure 2.[11–14]
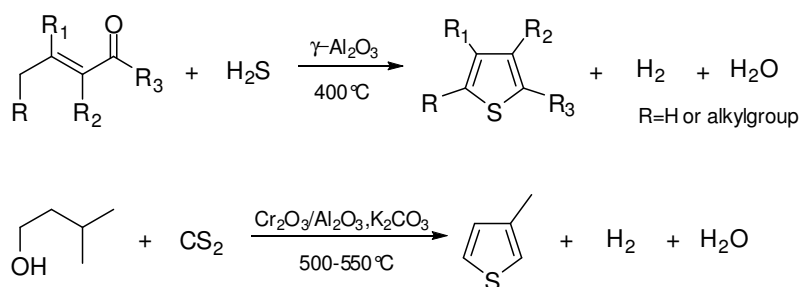


Figure 2. Some examples of cyclization reactions

One example of the flow sheet of a vapor phase process is reported in Figure 3. The reaction are performed in multitubular fixed bed reactors operating at atmospheric pressure or up to $10^3$kPa and maintaining a temperature comprised by 400-500°C. The process effluent is condensed and the desired product is separated by distillation from the low boiling compounds and the small amount of high boiling tar. Waste gases are combusted giving a single discharge.[3]
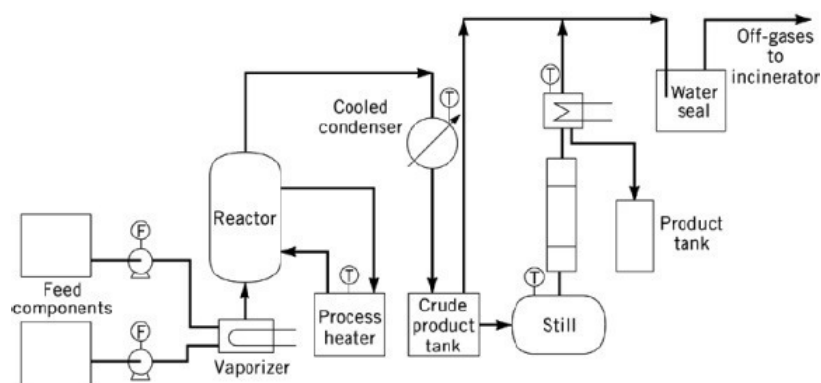
Figure 3. Schematic diagram of a typical plant for the vapor phase synthesis of thiophene and alkylthiophenes.[3]

Some other synthesis using different reactants are known, Scheme 1: (a) reaction between 1,4-dicarbonyl compounds and phosphorous sulfides (Paal Synthesis); (b) condensation of 1,2-dicarbonyl compounds with thio-diacetates (Hinsberg Synthesis), and (c) reaction of thioglycolates with 1,3-dicarbonyl compounds can be cited as example. However the formation of a very complex mixture of products makes all these processes not suitable for a large scale production.[1,2]
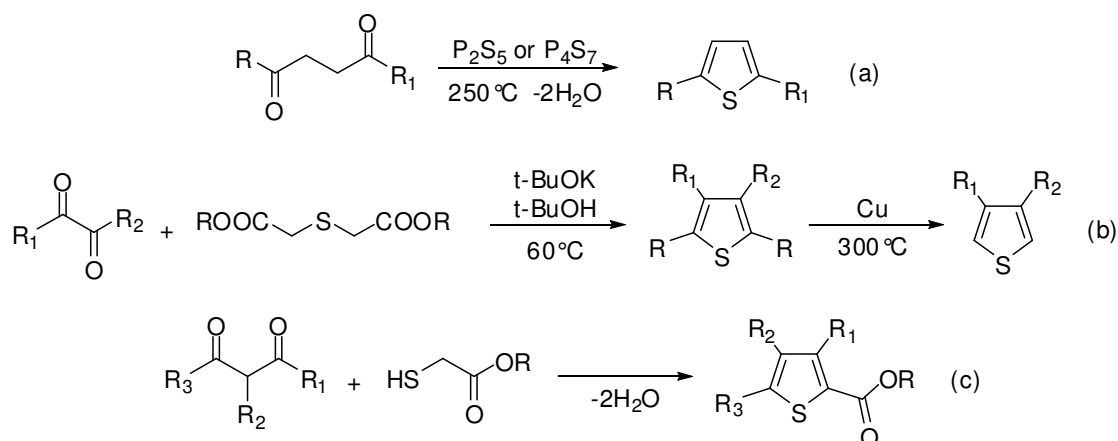


Scheme 1. Different methods for the synthesis of thiophene derivatives. (a) From 1,4 - Dicarbonyl Compounds and phosphorous sulfide (Paal Synthesis); (b) From Thiodiacetates and 1,2 - Dicarbonyl Compounds (Hinsberg Synthesis); (c) From Thioglycolates and 1,3 - Dicarbonyl Compounds

Electrophilic substitution at carbon atom represents an alternative route to obtain functionalized thiophene compounds, but positional selectivity of the attack must be evaluated carefully. It is well known from the literature that electrophilic substitution in heteroaromatic compounds occurs through a mechanism similar to the one of benzene, with the formation of a sigma-complex. Considering the stability of the transition state it is possible to explain the different reactivity of 2 and 3-position: as shown in Scheme 2, the attack in 2-position results in an higher

stability of the corresponding transition state (higher number of resonating structures) then electrophilic attack at 2-position is favored.
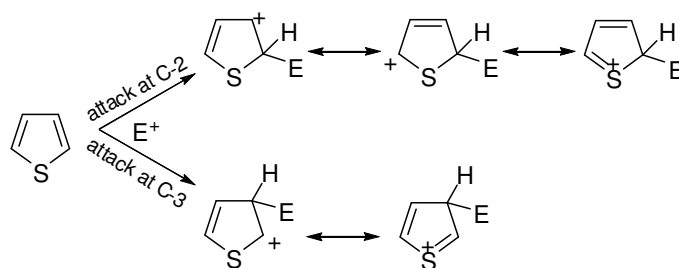


Scheme 2. Electrophilc attack at C atom, relative stability of σ-complex

The 2:3 isomer ratio depends both on the nature of the electrophiles and the reaction temperature. Further functionalization of the ring must to take into account the directing effect of the substituents already attached on thiophene, a detailed investigation on factors controlling positional selectivities of electrophilic substitution on heteroaromatic compounds has been carried out by Belen'kii *et al.*[15,16] Summarizing the results, it follows that with the position 2 occupied by an activating group (-R, -X, -OR, -NH$_2$, -NHR) the second attack occurs in 5-position; whereas the presence of a deactivating group (-NO$_2$, -CN,-COR) in 2-position directs the second substitution in position-4.

Processes for the synthesis of more than 50% of thiophene derivatives are based on Friedel-Crafts acylation. The main reason is that the reaction occurs exclusively at 2-position (2:3=200:1), moreover interesting results have been achieved in the replacement of conventional processes carried out in presence of metal halides or strong protic acids with new and greener ones based on solid acid catalysts. For example, Choudary *et al.*[17] reported the liquid phase acetylation of thiophene using acetic anhydride in presence of metal-exchanged (Fe$^{3+}$ and Zn$^{2+}$) K10 clay at 80°C. The reaction occurs selectively at 2-position (selectivity of 99%) reaching a conversion higher than 90%. Beta zeolite showed very good results in acylation of thiophene, 2- and 3-methylthiophenes with acetic anhydride at 60°C. In all tests the only product observed was the α-monoacylated (positions 2 or 5).[18] Finally, Isaev *et al.*[19] investigate the role of Lewis and Bronsted acid sites of different zeolites (HZSM5, HMOR, USY, and HY) in the acylation of thiophene with butyryl chloride.

Alkylation of thiophene occurs readily but monalkylated product, activated by the presence of the alkyl group, undergo polyalkylation and polymerization quickly, resulting in the loss of selectivity. Furthermore alkylation does not proceed only in 2-position as in case of acylation, but a mixture of 2 and 3-isomer is always obtained. For this reason alkylated thiophene compounds, which are valuable intermediates for the production of fine chemicals, are mainly synthesized using cyclization reactions or acylation followed by Clemmensen (acidic condition,

Zn(Hg) in HCl) or Wolff-Kishner[20,21] (basic condition, NH$_2$NH$_2$/KOH) reduction of the carbonyl group. Catalytic reduction has also been performed in presence of tungsten-nickel catalyst,[22] cobalt polysulfide[23] and cobalt octacarbonyl [Co$_2$(CO)$_8$].[24] Acylation proceeds selectively in 2-postion, then the as formed compound may be reduced to the corresponding 2-alkyl thiophene. 5-position is now activated by the presence of the alkyl group and a second acylation step will result in the selective formation of 2-alkyl-5-acyl thiophene, which can be eventually further reduced giving 2,5-dialkyl thiophene. This synthetic procedure has a limitation: carbon atom of aliphatic chain directly linked to thiophene must be unsubstituted. An example of useful compound, mainly used in fragrances industries, which cannot be synthesized *via* acylation is the 2-isopropylthiophene. An alternative route on lab scale is the reaction of 2-acetylthiophene with CH$_3$MgCl, Grignard reagent, to give 2-(thiophen-2-yl)propan-2-ol, which is converted in the desired product by palladium catalyzed dehydration-hydrogenation reactions.
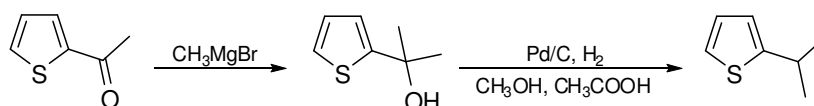


Scheme 3

The above-described synthetic procedures are based on multi-step and sometimes stoichiometric reaction sequences and involve the use of reactants, such as Grignard reagents, which are highly unstable and require many handling precautions. The development of new processes based on direct alkylation of the ring can overcome these problems.

Few papers concerning direct alkylation of thiophene with alcohols and alkenes have been published, in all cases very poor yields and low selectivities in the desired isomer have been obtained. On the basis of the reported results it is clear that low yields may be mainly attributed to undesired polymerization reactions, whereas the control on the product distribution, and in particular the control on the 2:3 isomer ratio remains still unclear. Benzylation of thiophene using K10 montmorillimite clays, modified with either Zn(II) or Fe(II) chloride as catalyst has been performed in liquid phase, using chlorobenzene, dichloromethane or nitrobenzene as solvent. Reaction occurs predominantly in 2-position, but the amount of 3-benzylated product increases with reaction time, in particular the 2:3 isomer ratio decreases from 2.7 to 2.0 in one hour. Authors suggest that a rearrangement of the kinetic product, 2-isomer, to the more thermodynamically stable product, 3-isomer, occurs.[25] Appleby *et al.*[26] reported that gas phase alkylation of thiophene with propylene catalyzed by phosphoric acid supported on kieselguhr proceed with the formation of 2- and 3-isomer in molar ratio of 1.44. The relative amounts of the two isomer were not affected by changes in operating

pressure, in thiophene/alkylating agent molar ratio and in weight space velocity, differently from results reported for benzylation of thiophene.[25] Eichler *et al.*[27] studied the possibility to obtain 3-alkylthiophens by vapor phase isomerization of the 2-isomer using different zeolites as catalyst, with pentasil zeolites being the most efficient ones. On HZSM5 at 330°C 2-methylthiophene were converted into 3-methylthiophene, with a 2:3 isomer ratio of about 1.38, small amounts of thiophene and dimethylthiophenes were also detected. Note that, the isomer distribution is almost the same to the one obtained through direct alkylation of the ring. Transformation of 2-alkylthiophenes on oxide, sulfide and zeolite catalysts were studied by Mashkina *et al.*[28] Acid catalysts, such as amorphous aluminosilicalite and zeolites in the hydrogen form, were the most active in dealkylation of 2-alkylthiophene, simultaneously isomerization and cracking reactions occurred. Summarizing, it has been observed that literature concerning thiophene alkylation is dated and in most of cases contradictories results were reported without any satisfactory explanations. Most recent works about thiophene alkylation focused on the removal of sulfured molecules from FCC without giving any particular attentions to the selective production of a particular alkylthiophene; then reported information are not useful in order to better clarify the reaction pathway. From these few studies emerge that the influence of the reaction parameters on the product distribution of the reaction is not clearly understood and requires a deeper investigation due to the high complexity of the reaction. Since direct alkylation represents a very attractive alternative for the synthesis of alkylthiophene, we decided to further investigate the role of all the factors which are involved in the reaction.

# EXPERIMENTAL

*Materials.* Thiophene (>99%) and 2-propanol (99,5%) were purchased from Aldrich Chemicals and used without further purification.

Five commercial catalysts were investigated: $SiO_2$ (Devicat Si 1402, Grace), $\gamma$-$Al_2O_3$ (Sasol), beta zeolite (PB Zeocat, HBEA), pentasil zeolite HZSM5 (Zeocat PZ), and acid-treated clay (Engelhard, F-13).

*Catalytic Tests.* Before the tests all catalysts were calcined for 6 h at 500 °C. Catalytic tests were carried out at atmospheric pressure in a fixed bed continuous flow reactor (length 390 mm and inner diameter 8 mm) using $N_2$ as the carrier gas (Figure 4) varying the contact time in the range 0.005-10 s (0.005, 0.05, 1, 3, and 10 s). The reactor was charged with 1 $cm^3$ (particle size 40-60 mesh) of fresh catalyst, then catalytic runs were performed at different temperatures, 200 and 300 °C. Thiophene was fed using a syringe pump and vaporized into a preheated flow of $N_2$ and propylene (alkylating agent); propylene flow was set to reach a 1:3 or 3:1 molar ratio of thiophene to propylene, depending on the test. In the test performed using

2-propanol, the thiophene/2-propanol (1:3 mole ratio) mixture was fed using a syringe pump and vaporized into a preheated flow of $N_2$.
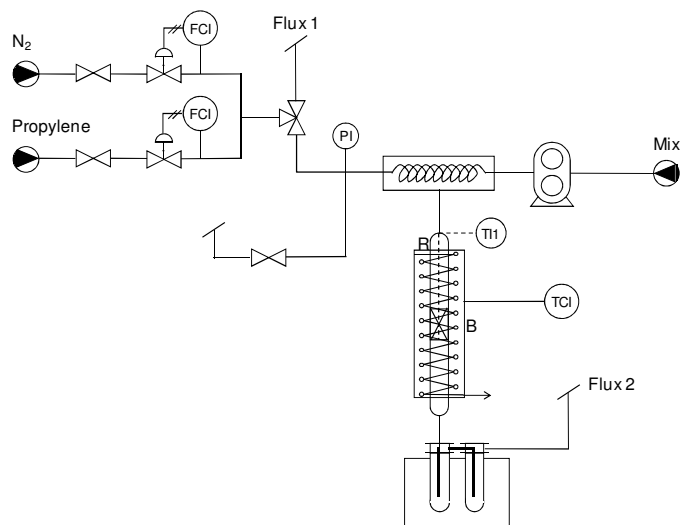


Figure 4. Schematic representation of the lab plant.

In the adsorption-desorption test, thiophene (0.9 ml/h) was vaporized into a preheated $N_2$ flow and fed over 1 cm$^3$ of HBEA for 1 h at 300°C, then thiophene feeding was stopped and the thiophene concentration in the outlet stream was monitored for the further 8 h.

Pulse-adsorption experiment was performed feeding the mixture thiophene/propylene (1:3 mole ratio) for 15 minutes, then thiophene feeding (0.9 ml/h) was stopped and only propylene was flushed for 30 minutes over the catalyst. This pulse sequence was repeated three times.

In all tests $N_2$ flow was set to reach a 9:1 volume ratio of $N_2$ to reactants mixture (thiophene and alkylating agent or only thiophene depending on the test).

During the catalytic tests the outlet stream was condensed in HPLC-grade acetone cooled in an ice bath at 0 °C, the obtained solutions were analyzed using a Carlo Erba 4300 gas chromatograph, equipped with FID and a HP-5 column (length 30 m, i.d. 0.32 mm, film width 0.25 μm) and identified by GC-MS using an AgilentTechnology 6890N equipped with a 5973 mass selective detector and an HP5 column (length 25 m, i.d. 0.25 mm, film width 1.5 μm). Products concentration were calculated using undecane as internal standard.

*Characterization.* Ammonia-Temperature Programme Desorption ($NH_3$-TPD). Acid properties of the catalysts have been evaluated by means of temperature programmed desorption (TPD) of $NH_3$ using a Termoquest TPDRO instrument. Approximately 120 mg of the catalyst sample were pretreated in He flow (20 ml/min) at 500 °C for 1 h. The sample was then cooled to 200 °C and flushed with 10% $NH_3$/He (20 ml/min) until saturation. Physically adsorbed $NH_3$ was eliminate

purging the sample with He (20 ml/min) for 30 minutes. The sample was then heated to 500 °C at a rate of 10 °C/min, simultaneously $NH_3$ desorption was continuously monitored by TCD detector.

# RESULTS AND DISCUSSION

The literature overview suggest that the development of a one-step heterogeneous process for the direct functionalization of thiophene ring through alkylation represents a challenge. In this field, the contradictory literature results may be not due to the infeasibility of the reaction but to the inadequate investigation of the reaction mechanism. Then a deep analysis of the critical step seems to be the only one possibility to clarify the nature of the apparently strange chemistry of this reaction. In order to achieve this goal the role of each "character", involved in the reaction, has to be attributed. The impact of this research, even if the selectivity and yield values in 2-isomer will be not sufficiently high to justify the development of an industrial process, will be helpful for future scientific studies.

## Role of the catalyst

It is well known from the literature that, most of conventional homogeneous alkylation processes have been replaced with heterogeneous ones based on solid acid catalyst, such as zeolites, clays and related materials. Based on these considerations, preliminary tests on different classes of materials have been performed in order to identify the suitable catalytic material for further investigation. Five solid catalysts with different acid-base properties were tested in the isopropylation of thiophene using propylene: $SiO_2$, characterized by the presence of weak Bronsted sites; γ-$Al_2O_3$, which exhibits primarily Lewis sites; HBEA and HZSM5, stronger acids with both Bronsted and Lewis sites; acid-treated clay (F13), which has a comparable acidity but a completely different framework. HBEA and HZSM5, were tested in order to evaluate the effect of the different channel network. Summarizing the choice of these five catalysts allows us to investigate the role of: (i) strength, (ii) distribution, (iii) type of the acid sites, and (iv) catalyst morphology. Reaction were performed with a contact time of 1 s and using a 1:3 thiophene to propylene mole ratio, the obtained results are shown in Table 1. As it is possible to see conversion values of thiophene are not reported, because its concentration in the outlet stream showed a strange trend, probably due to a strong and irregular adsorption/desorption phenomena on the catalyst surface. This latter behavior has not been observed before and does not allow the calculation of both the conversion and the balance.

Table 1. Acidity and activity of the tested samples, 300 °C, 1s, th/propylene = 1:3 mol/mol.

| catalyst | acid amount (mmol NH$_3$/g$_{cat}$) | 2-isomer, yield | 2:3 isomer ratio |
|----------|---------------------------------------|-----------------|------------------|
| γ-Al2O3  | 0.05 | 0  | -    |
| SiO2     | 0.04 | 0  | -    |
| HBEA     | 0.5  | 15 | 1.38 |
| HZSM5    | 0.5  | 11 | 1.38 |
| F-13     | 0.4  | 10 | 1.41 |

Yield values are calculated at t = 2h

Reported results show that γ-Al$_2$O$_3$ and SiO$_2$ were totally inactive, whereas yields in the 2-isomer around 10-15% has been observed in case of zeolites and acid treated clay. All tests showed the same trend in term of products yields, as example in Figure 5 are plotted results obtained in the test HBEA τ = 1 s. It is important to note that 2:3 isomer ratio is not effected by changing the catalysts and remains constant for the duration of the test.
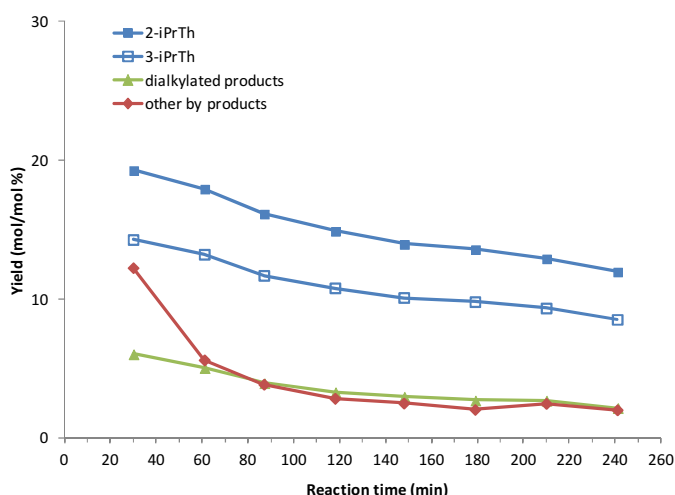


Figure 5. Yields of 2-, 3-isopropylthiophene, diisopropylthiophenes, and others by products as a function of time on stream.

In all the performed tests, the analysis of the condensed outlet stream showed the formation of very complex mixture of products, side reactions such as polymerization and cracking occurs. Together with 2- and 3-isopropylthiophenes, 2- and 3-methyl and ethylthiophenes, diisopropilthiophenes, naphatelene, 2,3-dihydrobenzo[b]thiophene, benzothiophene, alkylbenzothiophenes and low weight thiophene oligomers were also formed. Since HBEA showed best performance, further investigation on the other reaction parameters has been performed on this sample.

### Role of alkylating agent

The role of alkylation agent has been evaluated using 2-propanol instead of propylene, maintaining a reaction temperature of 300 °C and a contact time of 1s. The result of the test is reported in Table 2, no differences between the two reactants have been observed. From an economic viewpoint the use of propylene gives advantages deriving from its lower price and easier separation from reaction mixture, then further tests were performed using propylene. Furthermore the use of propylene gives advantages also on laboratory scale, avoiding the problems in reagents evaporation and products separation.

Table 2. Reaction conditions: HBEA catalyst, 1 s, 300 °C, th/alkylating agent = 1:3 mol/mol.

| alkylating agent | 2-isomer, yield | 2:3 isomer ratio |
|---|---|---|
| propylene | 15 | 1.38 |
| 2-propanol | 14 | 1.38 |

Yield values are calculated at t = 2h

### Role of feed composition

As shown in Table 3, the relative amount of 2- and 3-isopropylthiophenes was not markedly affected by the increase of the thiophene/propylene mole ratio from 1/3 to 3/1, small decrease in 2-isomer yield was observed.

Table 3. Reaction conditions: HBEA catalyst, 1 s, 300 °C.

| thiophene/propylene molar ratio | 2-isomer, yield | 2:3 isomer ratio |
|---|---|---|
| 1/3 | 15 | 1.38 |
| 3/1 | 11 | 1.36 |

Yield values are calculated at t = 2h

### Role of the temperature

2-Isopropylthiophene formation is favored at low temperature, but its yield is clearly lower. The enhancement in the selectivity of the 2-isomer is not enough to justify the high loss of yield.

Table 4. Reaction conditions: HBEA catalyst, 1 s, th/propylene = 1:3 mol/mol.

| Temperature (°C) | 2-isomer, yield | 2:3 isomer ratio |
|---|---|---|
| 200 | 8 | 1.47 |
| 300 | 15 | 1.38 |

Yield values are calculated at t = 2h

## Role of contact time

The influence of the contact time on the products distribution were finally evaluated, performing the reaction in the optimized reaction conditions, 300°C and thiophene/propylene mole ratio of 1/3.

Table 5. Reaction conditions: HBEA catalyst, 1 s, 300 °C, th/propylene = 1:3 mol/mol.

| contact time (s) | 2-isomer, yield | 2:3 isomer ratio |
|---|---|---|
| 0.005 | 4 | 1.38 |
| 0.05 | 7 | 1.38 |
| 0.5 | 14 | 1.38 |
| 1 | 15 | 1.38 |
| 3 | 16 | 1.35 |
| 10 | 16 | 1.33 |

Yield values are calculated at t = 2h

Considering that the relative amount and the yields of the 2- and 3- isomers are not highly affected by changing the contact time from 0.5 to 3 seconds, we decided to extend the range from 0.005 to 10 seconds. Despite the decreasing of the contact time until 0.005 s, no change in the 2:3 isomer molar ratio were observed. A very small difference, around 3.6%, in the ratio was obtained increasing the contact time until 10 s. On the basis of the obtained results it is clear that this unusual reaction proceeding may be mainly attributed to the fluid dynamics, such as extra and intra diffusion phenomena, and to some other factors related to the thiophene properties rather than to the chemistry of the reaction (kinetic and thermodynamic). The tests usually performed to verify the presence of any mass transfer limitations can not be conducted in this case because of the impossibility to calculate the thiophene conversion. Then alternatively tests were performed as reported below.

Adsorption-desorption experiment at 300 °C was performed in order to confirm the strong interaction of thiophene with the catalyst: HBEA was exposed to a thiophene/$N_2$ stream (1:9 volume ratio) for 1h, then the thiophene feed was stopped and the sample was flushed for 8 hours with pure $N_2$. Thiophene adsorption on HBEA was around 40%, then thiophene desorption started and continued for all the duration of the test.

Considering that a large amount of thiophene molecules are retained on the zeolite surface we decided to investigate the reactivity of these molecules in presence of propylene.

## Pulse-test

The removal of adsorbed thiophene via reaction or desorption was examined using a propylene stream, obtained results are reported in Table 6. Thiophene adsorbed on catalyst surface reacted with propylene to give a product mixture enriched in the 2-isomer.

Table 6. Pulse test on HBEA at 300 °C. Feed: (i) mixture thiophene/propylene (1:3 mole ratio) for 15 minutes, then (ii) only propylene was flushed for 30 minutes over the catalyst. These two steps were repeated 3 times.

| feed composition (reactant/$N_2$) | 2:3 isomer ratio |
| --- | --- |
| Th/Propylene | 1.35 |
| **Propylene** | **1.58** |
| Th/Propylene | 1.35 |
| **Propylene** | **1.54** |
| Th/Propylene | 1.36 |
| **Propylene** | **1.57** |

The possibility to slight change the 2:3 isomer ratio is evidenced by the obtained results, but before deeply discuss the reasons of this behavior it is necessary to analyze some interesting aspects reported in literature.

Several papers concerning thiophene adsorption and reaction on zeolite have been published, in particular the possibility to reduce the sulfur content from FCC through selective removal or cracking of organosulfur compounds on zeolites has been studied.[29–33] Chica *et al.*[29,30] reported a detailed investigation concerning thiophene behaviour on HZSM5 an HY, a kinetic model about catalytic conversion of thiophene on HZSM5 has been reported by Jaimes *et al.*[33] Results show oligomerization and adsorption on Bronsted acid sites occurs. Adsorbed thiophene undergoes ring-opening with consequent formation of $H_2S$ and butenes. The formed unsatured fragments may react with thiophene molecules, resulting in the formation of $C_4$-alkylatedthiophenes (Figure 6a.1). These latter compounds may undergo both cyclization reaction giving benzothiophene and cracking (before hydrogen transfer step) giving 2-methylthiophene and propene (Figure 6a.2-3-4). Thiophene may also be protonated and undergoes alkylation with olefins, which derives from cracking reactions (Figure 6b). All these reactions are responsible for the very complex mixture of products observed in the outlet stream. A similar mechanism for thiophene cracking on USY zeolite has been reported by Shan *et al.*[31] These results are in accordance with FT-IR and UV-Vis spectroscopic investigations,[34–36] reported results show the formation on hydrogen bonded complex with the π-electron system of thiophene which undergoes protonation and then oligomerizations.
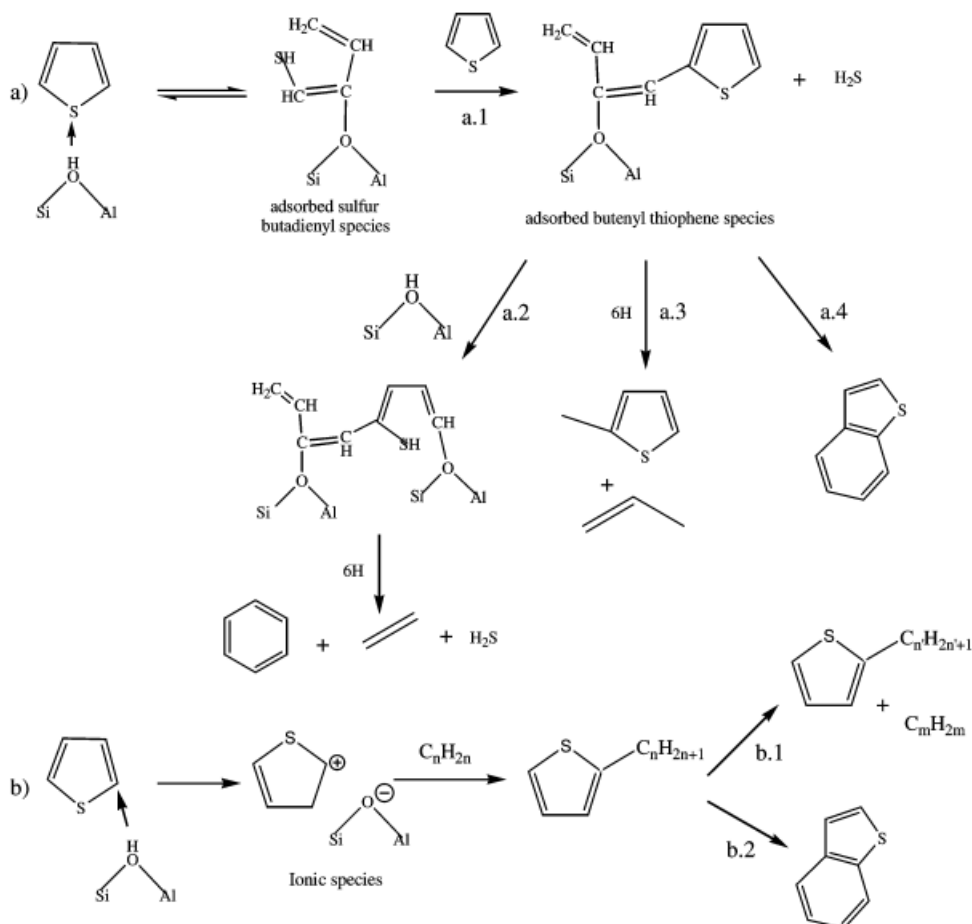
Figure 6. Reaction scheme of thiophene on HZSM5: (a) ring-opening and formation of butenylthiophene intermediates (b) thiophene protonation and alkylation.[33]

The adsorption/desorption behavior and the reactivity of adsorbed thiophene molecules evidenced by several authors are in accordance with the catalytic data reported above and are able to explain the formation of observed mixture of products. Moreover on the basis of these considerations the above reported results about the products distribution require a careful evaluation.

Alkylation of thiophene leads to the formation of two monoalkylated products: the 2-isomer which is the kinetic product and the 3-isomer, the thermodynamic one. As expected, at low temperature the kinetic product is favored, thus 2:3 isomer mole ratio increases from 1.38 to 1.47 decreasing the temperature from 300 °C to 200 °C. Another way to promote the formation of the kinetic product is the reduction of the contact time, but results show that the 2:3 isomer ratio remains unchanged despite the decrease of the reaction time from 3 s to 0.005 s. It is necessary to increase the residence time until 10 s to observe a small enhancement in the 3-isomer yield, 2:3 isomer mole ratio decreased from 1.38 to 1.33, but the kinetic product still dominates. Longer reaction time will shift the equilibrium further toward the most stable product, whereas it seems that the possibility to further increase the selectivity of the 2-isomer is affected by a diffusion process which limit the effect of lowering the reaction time.

Considering the high adsorption of thiophene it is possible to hypothesize that catalytic sites are quickly saturated, with a consequent formation of a chemically bonded thiophene layer. This latter phenomenon results in the "loss of significance" of the contact time, the presence of the film do not ensure a uniform residence time of the inlet flow molecules. The effective contact time of the molecules which are really involved in the reaction, the ones that constitute the film, is longer respect the theoretical one. Once the saturation is achieved, differences in the thiophene inlet flow, then in the residence time, do not have any influence in the reaction proceeding. The saturation of the caltalytic sites represent the critical step of the reaction is controlled by the rate of diffusion of the reactants, mainly propylene, through the film.

Proposed mechanism is schematized below. In the tests performed at a contact time smaller than 3 s, the thiophene flow is sufficiently high to saturate the catalyst surface in very short times, with the consequent formation of the chemically bonded thiophene layer. At this point propylene molecules must pass through the film in order to react with adsorbed thiophene molecules and the inlet flow rate do not have any influence on the reaction proceeding. This is the reason why no differences in product distribution have been observed operating in the range 0.005 to 3 s.

The results of the pulse test are in accordance with the just described situation, this test may allow to simulate the effect of lowering the contact time if the saturation of the catalyst surface would not been achieved. The first 15 minutes are performed at a contact time of 1 s, then as expected the 2- and 3-isomers are produced in the same molar ratio as before: the reaction is limited by rate diffusion and mass transfer through the formed film. When thiophene feed was stopped, the adsorbed thiophene molecules partially desorbed and partially reacted with propylene to give the desired products. Thiophene layer is gradually removed and diffusion of the propylene is no more hindered by either other molecules or physical hindrances, then the mass transferring steps do not affect the reaction rate. In this situation it is possible to see the effect of lowering the contact time: the selectivity of the 2-isopropylthiophene increase, 2:3 mole ratio became higher than 1.5.

A different scenario occurs when operating at very high contact time, such as 10 s. In this case, the inlet flow is such slow that saturation of catalyst surface occurs slowly, moreover the residence time of propylene on the catalyst surface is sufficiently long to further shift the reaction equilibrium trough the thermodynamic product (3-isomer). Oversimplified graphic representation of the hypothesized phenomena on the catalyst surface are reported in Figure 7, and in Figure 8.

$$0.005 < \tau_{set} < 3 \text{ s}$$

CHEMICALLY BONDED
THIOPHENE LAYER

CATALYST SURFACE

2:3 ~ 1.38

$\tau_{apparent} \sim 3 \text{ s}$
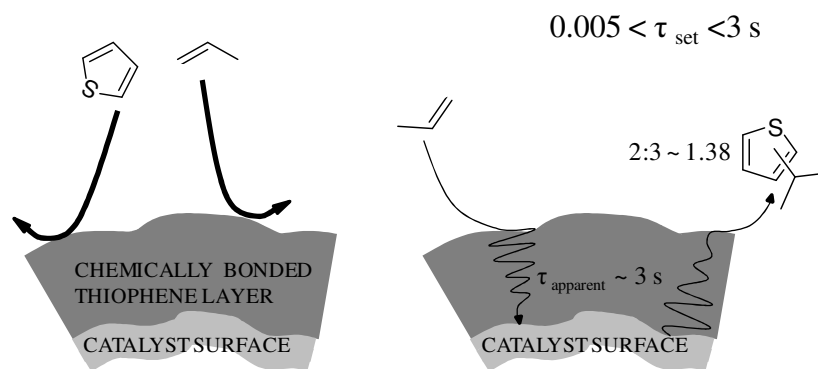
CATALYST SURFACE

Figure 7. Contact time comprised between 0.005 and 3 s. (Left) Thiophene molecules are strongly chemibonded on the catalyst surface, with the consequent formation of a layer. Thikness of the film may not be reduced by increasing the flow rate. (Right) The reaction proceeding is controlled by the rate of diffusion of the propylene and of the products mixture through the film.

When operating at a contact time lower than 3 s, as reported in Figure 7, thiophene molecules quickly cover the entire catalyst surface with the consequent formation of a chemically bonded layer. Before reacting propylene have diffuse through the layer, and reach some catalytic sites; then products have to retro-diffuse into the flow. The rate of these steps are limited by the presence of the thiophene layer. the thickness of the layer, and consequently the effective contact, can not be modified by increasing the rate flow due to the chemical nature of the interaction between thiophene and the catalytic surface.

Pulse test

2:3 > 1.50

$\tau_{set} = \tau_{apparent} < 3 \text{ s}$

CATALYST SURFACE
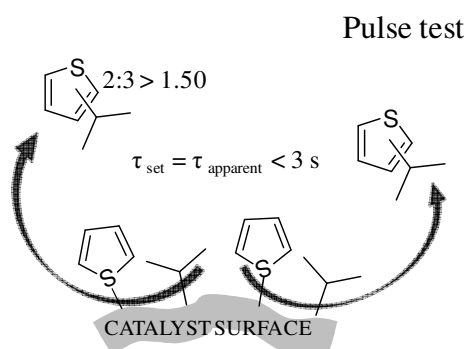
Figure 8. Pulse test, after stopping thiophene flow. The layer was eroded and the reaction is under kinetic control, selectivity of the 2-isomer increased.

In the case of pulse test, Figure 8, when the mixture is fed, the reactivity may be explained as before, but when thiophene flow is stopped the layer is progressively eroded by reaction with propylene. In this phase the reaction rate became limited by kinetic control, resulting in the increase of the kinetic product, 2-isomer.

# CONCLUSIONS

Gas phase isopropylation of thiophene has been investigated in order to elucidate the possibility to control the final products distribution by tuning the reaction parameters. In particular, attention has been focused on the possibility to shift the equilibrium toward one of the two isomers. The comprehension of thiophene behavior on catalyst surface allowed to understand the strange reactivity of thiophene in alkylation reaction. Results showed that reactivity of thiophene on solid acid catalyst is mainly affected by the strong adsorption on catalytic sites and the critical step of the reaction is represented by the formation of a thiophene shell on the catalyst surface. It is possible to hypothesize that control of regio-selectivity of the reaction is prevented by the hindrance of the thiophene layer, as confirmed by results obtained when operating at low contact time. Difficulties in changing product distribution have been already observed in literature but no one gave a reasonable explanation for this strange behavior, hence contradictory data have been reported.

The interest in developing a large scale process based on direct thiophene alkylation is further limited by the large numbers of simultaneous and consecutive reactions which are involved in the overall-process. These side reactions are responsible for the formation of a very complex products mixture and consequent difficulties in products purification.

Despite the impossibility of a large scale process development, we have clarify important mechanistic aspects of the reaction.

# REFERENCES

(1)     Swantston, J. In *Ullmann's Encyclopedia of Industrial Chemistry*; Wiley-VCH, W., Ed.; 2006; Vol. 5 Suppl 1.

(2)     Joule, J. A.; Mills, K. In *Heterocyclic Chemistry*; A John Wiley & Sons, Ltd., Publication, 2010; pp. 325-342.

(3)     Fuller, L. S. Thiophene and Thiophene Derivatives. *Kirk-Othmer Encyclopedia of Chemical Technology*; John Wiley & Sons, Inc., 2000.

(4)     Sum, P.-E.; Joseph, J. P.; Moan, C. B.; Lin, Y.-I. *Piperazine derivatives*, US Patent 5,210,193 1993.

(5)     Brooks, D. W.; Kerkman, D.; Martin, J. G.; Stewart, A. O.; Summers, J. B. *Urea based lipoxygenase inhibiting compounds*, US Patent 5,185,363 1993.

(6)     Bagli, J. F.; Ferdinandi, E. *Thiophene ethanolamines*, US Patent 4,105,663 1978.

(7)     Maidenhead, G. T.; Sanohurst, I. H. A.; Maidenhead, A. W. *Fungicides*, US Patent 6,123,356 2000.

(8)     Berglund, R. A. *Intermediate useful for the asymmetric synthesis of Duloxetine*, US Patent 5,491,243 1996.

(9)     Shepherd, R. G. *Hypolipidemic and antiatherosclerotic novel 4-(aralkyl-and heteroarylalkylamino)phenylcompounds*, US Patent4,211,783 1980.

(10)    Turin, L. *Lily of the valley aromachemicals*, US Patent 2005/0006476 A1 2005.

(11)    Bell, T. R.; Smith, P. G. *Continuous production of thiophene from butane*, US Patent 3,939,179 1976.

(12)    Clark, N. R.; Webster, W. E. *Synthesis of thiophenes*, GB Patent 1,345,203 1971.

(13)    Aquitaine, S. N. E. *Process for preparing thiophenes*, GB Patent 1,585,647 1977.

(14)    Clark, N. R.; Webster, W. E. *Synthesis of thiophenes*, US Patent 3,822,289 1974.

(15)    Belen'kii, L. I.; Suslov, I. A.; Chuvylkin, N. D. *Chem. Heterocycl. Compd.* **2003**, *39*, 36-48.

(16)    Belen'kii, L. I. *Heterocycles* **1994**, *37*, 2029-2049.

(17)    Choudary, B. M.; Sateesh, M.; Kantam, M. L.; Ranganath, K. V. S.; Raghavan, K. V. *Catal. Lett.* **2001**, *76*, 231–233.

(18)    Álvaro, V. F. .; Brigas, A. F.; Derouane, E. G.; Lourenço, J. P.; Santos, B. S. *J. Mol. Catal. A: Chem.* **2009**, *305*, 100–103.

(19)    Isaev, Y.; Fripiat, J. J. *J. Catal.* **1999**, *263*, 257-263.

(20)    Atsugi, S. M.; Yokohama, T. T.; Isehara, T. I.; Atsugi, Y. Y. *Mesomorphic compound, liquid crystal composition and liquid crystal device using same,* US Patent 5,118,441 1992.

(21)    Gubler, M.; Haap, W.; Hebeisen, P.; Kitas, E. A.; Kuhn, B.; Minder, R. E.; Schott, B.; Wessel, H. P. *New fbpase inhibitors for diabetes*, US Patent 2007/0281979 A1 2007.

(22)    Truitt, P.; Holst, E.; Sammons, G. *J. Org. Chem.* **1957**, *22*, 1107-1109.

(23)    Campaigne, E.; Diedrich, J. L. *J. Am. Chem. Soc.* **1951**, *73*, 5240-5243.

(24)    Greenfield, H.; Metlin, S.; Orchin, M.; Wender, I. *J. Org. Chem.* **1958**, *23*, 1054-1056.

(25)    Clark, P. D.; Kirk, A.; Kydd, R. A. *Catal. Lett.* **1994**, *25*, 163-168.

(26)    Appleby, W. G.; Sartor, A. F.; Lee Jr, S. H.; Kapranos, S. W. *J. Am. Chem. Soc.* **1948**, *70*, 1552–1555.

(27)    Eichler, K.; Ernst, I. L. *Process for isomerizing alkylthiophenes*, US Patent 4,783,541 1988.

(28)    Mashkina, a. V.; Chernov, V. I. *Kinet. Catal.* **2005**, *46*, 88-95.

(29)    Chica, A.; Strohmaier, K.; Iglesia, E. *Langmuir* **2004**, *20*, 10982-10991.

(30)    Chica, A.; Strohmaier, K. G.; Iglesia, E. *Appl. Catal., B* **2005**, *60*, 223–232.

(31)    Shan, H. H.; Li, C. Y.; Yang, C. H.; Zhao, H.; Zhao, B. Y.; Zhang, J. F. *Catal. Today* **2002**, *77*, 117–126.

(32)    Tian, F.; Wu, W.; Jiang, Z.; Liang, C.; Yang, Y.; Ying, P.; Sun, X.; Cai, T.; Li, C. *J. Colloid Interface Sci.* **2006**, *301*, 395-401.

(33)    Jaimes, L.; de Lasa, H. *Ind. Eng. Chem. Res.* **2009**, *48*, 7505-7516.

(34)    Garcia, C. L.; Lercher, J. A. *J. Phys. Chem.* **1992**, *96*, 2669–2675.

(35)    Spoto, G.; Geobaldo, F.; Bordiga, S.; Lamberti, C.; Scarano, D. *Top. Catal.* **1999**, *8*, 279-292.

(36)    Geobaldo, F.; Palomino, T.; Bordiga, S.; Fisica, C.; Giuria, V. P. *Phys. Chem. Chem. Phys.* **1999**, 561-569.

# Chapter 3

# Green production of aromatic aldehydes by direct selective oxidation of the corresponding alcohols

## INTRODUCTION

Gold in bulk form is known to be chemically inert and has been generally considered to be inactive material for catalysis. This idea started to changed when in 1973 Bond *et al.*[1] found that gold on silica, γ-alumina or bohemite may effectively catalyze the hydrogenation of alkenes and alkynes at relative low temperatures, 100-217 °C. But interest in using gold as catalyst drastically increased some years later after the pioneering discovery, made by Haruta and coworkers[2] in the 1980s, that finely dispersed gold nanoparticles are highly active in low-temperature CO oxidation. In particular at temperature significantly below 0 °C small gold nanoparticles, with diameter smaller than 5 nm, supported on α-$Fe_2O_3$ showed a high catalytic activity, which is not replicated by other metal. Moreover authors observed that method of preparation of the catalyst played an important role on the activity of the material. In a subsequent work Haruta[3] found that Au/$TiO_2$ was equally active in catalyzed the same reaction. In 1985 Hutchings[4] discovered that supported Au was the most active catalyst for the hydrochlorination of ethyne to vinyl chloride. These pioneering studies reported for the first time gold based materials to be the best catalysts for the considered reactions. The impact of these discoveries is testify by the exponent increase in the number of publications about gold catalysis over the past two decades.[5] Gold based catalysts were found to be active in many classes of reactions, such as liquid and gas phase oxidations, WGS reaction, decomposition of NOx, VOC reduction, and selective hydrogenations.[5–7]

It is widely accepted that catalytic properties of a metal are highly influenced by the particle size, however the reason for the unexpected gold nanostructured activity is still controversial and many researchers have been performed in order to understand the origin of this unique reactivity.

## Gold properties and reactivity

The tendency of a metal to bind oxygen dissociatively may be used as a measure of its nobility. Differently from the neighbor metals Au has an endothermic dissociative chemisorption energy (see Figure 1), which implies that $O_2$ does not dissociate on Au. This property has to be ascribed to the energy of the Au d-states.[8]

| Co | Ni | Cu |
|-------|-------|-------|
| -5.07 | -3.90 | -2.51 |
| Pd | Pd | Ag |
| -1.20 | -1.20 | -0.65 |
| Pt | Pt | **Au** |
| -2.17 | -2.17 | **+0.54** |

Figure 1. The dissociative chemisorption energies for oxygen on transition metalsurfaces with respect to a molecule in vacuum calculated by density functional theory (DFT).[8]

Due to the large mass of its nucleus the relativistic effects are very important for Au:[9–11] the s and p orbitals are contracted, whereas the d and f ones are expanded,[12] thus the 6s orbital is more contracted and stabilized. Au d state are so low in energy that they can not interact with 2p valence state, then $O_2$ does not dissociate on Au surface. This is in sharp contrast to the observed high activity of small nanoparticle in catalyzed CO oxidation. The reduction of particle size implies changes in d-states, which results in the decreasing of the adsorption energies and in the ability of Au to bind oxygen.[8,13]

## Particle size

Catalytic activity for CO oxidation of Au NPs supported on different metal oxides have been reported by Lopez *et al.*[13] Collected data show that the rate reaction for CO oxidation for particles smaller than 5 nm is by far higher than rate observed for 20-30 nm particles. This result clearly demonstrates that the role of the support, in term of charge and oxygen transfer, is important but the size of gold particle is the dominant effect. Moreover density functional theory calculation (DFT) have been performed[8,13] in order to investigate the effect of the coordination number of Au atoms on the chemical activity of the gold, Figure 2.
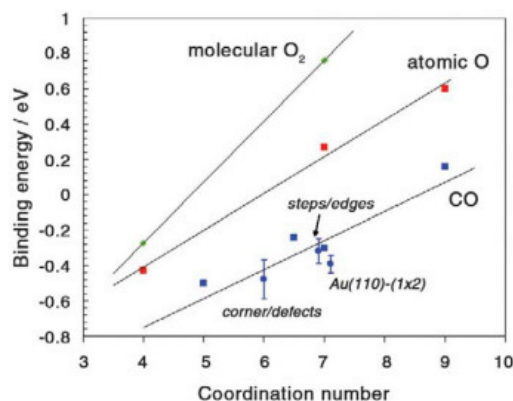
Figure 2. Relationship between binding energies for $O_2$, O, CO and coordination number of gold atoms in different surfaces and cluster.[8]

Coordination number decreases from 9 in surface Au atoms, to 7 in edge atoms and finally to 4 in corner ones. Results show that binding energies of CO and O decrease linearly whit the coordination number, then the lower coordinated atoms are the most active in catalyzing CO oxidation. The fraction of low-coordinated Au atoms, both edge and corner, increases significantly upon diminishing the particle size dimension, this coincides with the observed increase in the CO oxidation activity.[14] Moreover atoms at the perimeter sites, the ones in contact with the support, show significant differences in catalytic activity, and they probably play a paramount role in catalysis.[15–17]

## Interaction with the support: Au on $CeO_2$

Supported gold catalysts are prepared by loading the desired amount of metal, via deposition-precipitation, precipitation, coprecipitation or colloidal dispersion, onto different metal oxides, such as $TiO_2$, $CeO_2$, $Fe_2O_3$, $Al_2O_3$, $SiO_2$. The catalytic properties of the metal particles are strongly affected by the interaction with the support, then the choice of the most suitable oxide represent a key factor in the success of the reaction.[16] Generally the role of the support is to stabilize small particles during the preparation and further thermal treatments[15,18] but evidences for electronic effects on Au nanoparticles have been observed. Metallic oxides used as supports may be divided into "inert" and "active", depending of their redox properties. Then, $Fe_2O_3$ $TiO_2$ and $CeO_2$ are reducible transition metal oxides and have to be considered as "active", whereas $Al_2O_3$ and $SiO_2$ are "inert" supports because they are not able to supply reactive oxygen to the catalytic system. Among the reducible oxides, $CeO_2$ is one of the most efficient support because of its ability to store and release oxygen thorough a redox process involving $Ce^{4+}/Ce^{3+}$ couple. Highly mobile lattice oxygens are directly involved in the oxidation processes, this results in the formation of surface oxygen vacancies. Studies on ceria surface performed using both experimental and theoretical methods demonstrated that surface defects play a key role both in favoring the adsorption/dissociation of the

reactants on the surface (vacancies bind adsorbates strongly than normal oxide sites) and in promoting nobel metal activity.[19–24] In particular, considering gold catalysis many studies demonstrate that surface defects promote the nucleation and the stabilization of the Au particles. Redox processes involving lattice oxygens and surface species involved in CO oxidation have been been investigated by DRIFT and FTIR.[25] Despite the great effort to clarify the origin of such high activity of Au/CeO$_2$ catalyst, the nature of the active site is still unclear and is a matter of debate. Pillai and Deevi[26] attributed the high activity of Au/CeO$_2$ in CO oxidation to the presence of Au-OH$^+$ and Au$^0$ species highly dispersed and in strong contact with support defects. Several authors highlight the role of Au$^+$ and Au$^{3+}$ species,[27–30] others indicate that metallic sites are the active ones[31] whereas some results suggest a cooperative role of metallic and oxidized gold species.[32–34] Moreover other studies indicate that origins of the catalytic activity of Au/CeO$_2$ catalyst are related to complex interplay between the metal and the support: incorporation of gold cationic species into ceria lattice leads to the formation of modified mixed oxide Au$_x$-Ce$_{1-x}$O$_{2-\delta}$ with high redox activity.[35] A notable work of Corma[27] and co-workers reported the high activity of a gold catalyst supported on nanocrystalline CeO$_2$. A detailed spectroscopic investigation on the nature of the active sites and XPS analysis of this catalyst demonstrated that both cationic and metallic gold are present, and nanocrystalline CeO$_2$ supplies reactive oxygen in the form of surface peroxides and superoxide species. Enhance in activity is direct correlated with the Au$^{3+}$/Au$^0$ ratio increase. Other characteristics of the support that influence performance include surface area,[36–39] particle size and morphology.[40–42] Rolison and co-workers[37,38] proposed that comparability of the size allows individual Au particles to make contact with multiple domains of small sized support particles, resulting in the increase of the amount of the interfacial active sites. Advantages arising from the size effect of the supports have been investigated by Corma[39] and co-workers. Catalyst synthesized by supporting Au colloid on nanocrystalline CeO$_2$ ($\approx$ 5 nm) with a very high surface area, 180 m$^2$/g, was found to be two order of magnitude more active in CO oxidation then the catalyst prepared supporting Au on conventional CeO$_2$ (70 m$^2$/g) support. The same catalyst was tested in alcohol oxidation[43] giving best catalytic activity if compared with Au supported on conventional ceria, Au/TiO$_2$, Au/C and Au/Fe$_2$O$_3$.

## Au supported catalysts preparation

The properties of gold catalysts are strongly related to the preparation method, which strongly influences Au particle size. The precursors used in preparing supported gold catalysts are salts or complexes where gold is usually in +3 oxidation state (such as HAuCl$_4$·3H2O or AuCl$_3$), whereas few of them are in +1 oxidation state, that is more unstable. For most of the preparation methods gold is in +3 oxidation state after drying but it can be easily reduced to the metallic state by

thermal treatments which can be performed either in oxidizing or reducing atmospheres. Thermal treatments are often carried out in air, but it is very important to operate under controlled conditions because parameters, such as the nature of the gas, the flow rate, the final temperature, and the heating rate influence the particle size. The preparation method, the thermal treatment, and the nature of the support may also affect the morphology of the particles.

## Most used techniques

Many different techniques can be used in order to prepare highly dispersed gold catalyst and the choice of the most suitable one represent a key factor for obtaining a catalytic systems with good performances. Some of the most used techniques may be cited as example: impregnation, co-precipitation, deposition precipitation (DP), chemical vapor deposition (CVD), and immobilization of colloids.

Deposition-precipitation is the most widely used method for preparing active Au-based catalysts[14,44] and allow to obtain a supported catalyst with very small and highly dispersed Au particles. It consists in the selective deposition of $Au(OH)_3$ on the surface of the support by setting pH, temperature and concentration at the optimal values. The gradually raise of the pH of the solution in which the support is suspended cause the nucleation of the hydroxides or hydrated oxide on the support surface, and when properly performed, the whole active phase results attached to the support. There are different ways to deposit Au onto the support: either by adjusting the pH of $HAuCl_4$ with $Na_2CO_3$ or NaOH and then adding the support, or by slowly increasing the pH of the $HAuCl_4$ solution in the presence of the support.[45] This general procedure has many variations, such as pH, temperatures of preparation and washing and use of other bases, such as ammonia.[26,46–48] Some of these parameters have been systematically investigated; no significant differences were observed but there are often problems of reproducibility. Anyway it is claimed that very small Au particles are obtained, highly dispersed over the support.

Another common procedure is the immobilization of preformed Au colloids suspension. In this case the properties of the catalyst are strongly affected by the properties of the colloids. Numerous preparation methods have been developed to synthesized small colloidal gold particles. Most commonly ones are based on the reduction of gold salts in presence of a stabilizing agent, that prevent the particles aggregation.[49]

Colloidal solution of small Au NPs with a narrowed size distribution can be obtained by borohydride reduction of Au(III) in a traditional two phases system using a quaternary ammonium salt as phase transfer agent in presence of a ligands (such as alkylthiols, -amines, -silanes, etc.).[50] However, in order to obtain clean gold small nanoparticles, several purification steps (separation, decantation, filtration) are required, with a relevant loss of yield. Another common procedure is the reduction of a gold salt in aqueous solution using PVP, or a different water

soluble polymer as stabilizing agent. Albonetti and co-workers[51] patented a green approach for the synthesis of AuNPs by using non toxic β-glucose as reducing agent, they shown that heating a solution of gold precursor, PVP, and β-glucose activated by the presence of a base, results in the formation of small Au NPs (in the range 5-8 nm) in very short time. The main drawback in this kind of procedure is that the strongly bonded surfactant (PVP) is very hard to remove and may prevent the access to the catalytic site.

In order to overcome the aforementioned problems the investigation of novel and simple procedure for the synthesis of gold colloids represents one of the most attractive field of research. In the last few years the decomposition of organometallic precursor (Ru, Pt, Pd, …) in mild condition in presence of organic ligands as stabilizer has shown very attractive results,[52] but only few data on a similar approach for the synthesis of Au NPs are available. [53] Au(I) amino complex {Au[N(SiMe$_3$)$_2$]}$_4$ has been successfully used to prepare small gold nanoparticles on passivated silica under mild condition,[53] then it represent a suitable candidate for the synthesis of Au colloids via one pot decomposition of an organometallic precursor.

## Alcohol oxidation

The selective oxidation of alcohols is one of the most used reaction in organic chemistry both in laboratory and industrial scale because, the corresponding carbonyl compounds are important intermediates in the field of fine chemistry. In this field one of the most challenging tasking is the replacement of stoichiometric and highly toxic oxidizing agents such as permanganate and dichromate with heterogeneous and safety ones.[54] Attractive alternatively processes are based on direct oxidation of alcohol promoted by solid and reusable catalyst under mild and solvent free condition using O$_2$ or air at low pressure as oxidants. Satisfactory results have been attempted only in few cases, in which large excess of bases must be added with consequent loss in selectivity. For this reason the design of new catalysts able to promote the direct alcohol oxidation operating under mild condition represents a demanding tasking.

Gold based catalysts are suitable candidates in the research of the most active catalyst for aerobic alcohols oxidation. First studies performed by Rossi, Prati and co-workers[55,56] on this topic showed that supported gold nanoparticles are able to catalyze alcohols oxidation, whereas satisfactory results have been achieved only in present of a base, such as NaOH. Au supported on carbon in alkaline solution was found to be good catalyst for selective liquid phase oxidation of range of substrates, such as propanol, butanol and diols.[55] Furthermore Au/C showed good performances in the oxidation of D-glucose to D-gluconic.[56] Oxidation of D-glucose was also performed in presence of "naked" gold nanoparticles, results confirm the importance of the support in stabilizing metal particles.[57] More recently

Corma and co-workers[43,58] demonstrated that $Au/CeO_2$ catalysts are active also in base free condition. In particular they synthesized an Au supported on nanocrystalline $CeO_2$ catalyst able to catalyze alcohol oxidation in solvent free condition, without the addition of any bases, giving results comparable to the best ones previously reported by Kaneda et al.[59] using a Pd supported on hydroxyapatite catalyst. The same authors performed a kinetic study using benzyl alcohol as model substrate and proposed a molecular mechanism able to justify the catalytic results.[60] Very recently, Hutchings et al.[61] investigated the selective oxidation of benzyl alcohol to benzaldehyde using a Au supported in $CeO_2$ foam catalyst. Furthermore conversions of benzyl alcohol comparable to that of Pd-hydroxyapatite catalyst has been obtained using a Au supported on mesostructured Ga-Al mixed oxide catalyst.[62] A direct comparison among the catalytic performances reported in these studies is very hard because the reaction conditions vary drastically, but it seems that Au supported on $CeO_2$ represent a very promising catalyst for selective alcohols oxidation.

This short literature review shows that the innovative design of new active catalyst for the selective oxidation of alcohols has involved many effort owing to the important role of the carbonyl compounds as building block in fine chemical industry. Recently gold nanoparticles supported on $CeO_2$ were found to be promising catalysts for the development of new and environmentally friendly processes. Then in this work the attention has been focused on the investigation of the activity of a series of $Au/CeO_2$ catalysts prepared using different procedures in the liquid phase oxidation of aromatic alcohols under very mild conditions, low temperature and atmospheric air as oxidant. It is known that support particle size have a key role in enhancing catalytic performances of the catalyst. The best catalyst which has been reported in literature since now is the Au supported on nanocrystalline $CeO_2$ synthesized by Corma and co-workers.[43] then we decided to synthesize a nanocrystalline cerium oxide with a surface area comparable to the one of Corma, following a procedure similar to the one described in literature by Guo *et al.*[63] Then different amounts of gold were loaded on this support using two different techniques: deposition-precipitation and colloids deposition. Colloids suspension were synthesized by the glucose reduction of Au(III) in alkaline water in presence of PVP, under the optimized reaction conditions, using a conventional heating system. Furthermore, in the last part of the work we investigated the possibility to obtain small and narrow size-distributed Au NPs in a novel and simple way avoiding the use of tricky stabilizing agent *via* one pot decomposition of an organometallic precursor. For comparison, a similar series of samples were prepared by supporting gold on commercial $CeO_2$ support.

Our first studies focused on the investigation of the effects of preparation methods, gold loading and dispersion, and support particles size on the catalyst activity in

benzyl alcohol oxidation. Then the most active catalysts have been tested in the oxidation of piperonyl alcohol to piperonal.

In both cases the corresponding aldehydic compounds, benzaldehyde and piperonal, are valuable intermediate in the field of fine chemistry. Benzaldehyde is the second most important aromatic compound, after vanillin, used for cosmetic and flavoring applications. It is mainly produced through the hydrolysis of benzalchloride, derived from toluene chlorination, and as by-product in the air oxidation of toluene to benzoic acid.[64] Commercialization of benzaldehyde for perfumery and pharmaceutical industries required a high degree of purity, then organic chlorine or benzoic acid contaminations must be limited. Furthermore in order to meet the more stringent environmental regulations the development of new processes based on the direct selective oxidation of benzyl alcohol under mild condition represent a challenge target.

Piperonal (heliotropin or 3,4-(methy1enedioxy)benzaldehyde) is an important intermediates used in the synthesis of fragrances, cosmetics preparations, pharmaceutical and agrochemicals products.[65] Currently it is industrially prepared mainly by ozonolysis[66,67] or chromic acid[68] oxidation of isosafrole. These processes present several drawbacks in term of environmental pollution associated with chromium species, high cost related to the large amount of electricity necessary for ozonolysis and reduced availability of safrole which is isolated from the essential oil of Ocotea Cymbarum and Pretiosa trees. Some other synthetic routes starting from 1,2-methylendioxybenzene or 3,4-dihydroxybenzaldehyde are known, but these multistep processes are generally carried out in homogeneous system and required the use of highly toxic reactants, such as halogenated compounds.[69–71] Once considered the just mentioned problems, the development of alternative synthetic routes able to perform the direct oxidation of piperonyl alcohol with air at atmospheric pressure and low temperature may be identify as the final goal of this work.

# EXPERIMENTAL

*Materials.* $CeCl_3 \cdot 7H_2O$ (>99 %), $Ce(NO_3)_3 \cdot 6H_2O$ (>99 %), $CH_3(CH_2)_{11}OSO_3Na$ (>99 %), NaOH, PVP, β-D-glucose, $HAuCl_4 \cdot 3H_2O$ (>99,9%), AuCl (>99,9%), Lithium bis(trimethylsilyl)amide (LiHMDS) (97%), 0.1 M aqueous NaOH solution, toluene (CHROMASOLV® Plus, for HPLC, ≥99.9%), 1,2,4-trimethylbenzene (>99%), benzyl alcohol (>99%), 3,4-(Methylenedioxy)benzyl alcohol (or piperonyl alcohol, 98%), and undecane (>99%) were purchased from Sigma Aldrich and used without further purification. THF (Sigma Aldrich) was used immediately after drying and distillation over sodium-benzophenone under Ar atmosphere. The commercial $CeO_2$ used as support was purchased from Evonik (VP Ceria 60, Ce60).

*Synthesis of the High Surface area CeO₂.* High surface area CeO₂ samples (hsCe) were synthesized by surfactant-template method, following a procedure similar to the one reported by Guo *et al.*[63] using two different cerium precursors, CeCl₃·7H₂O and Ce(NO₃)₃·6H₂O (hsCe_Cl and hsCe_NO₃, respectively, see list of abbreviations below). Cerium precursor (27 mmol) was completely dissolved in distilled water (270 ml) and added dropwise to a water (105 ml) solution of dodecyl sodium sulfate (73 mmol). The obtained mixture was kept under vigorous stirring for 30 minutes, then a solution (160 ml) of NaOH (4.6 g) was added gradually. After 6 hours at RT under vigorous stirring, the mixture was transferred into a sealed vessel and submitted to microwave-hydrothermal treatment (110 °C 2 hours, rate 2 °C/min, 800 W) using a Milestone StartSYNTH microwave unit. The yellow precipitate was filtered, washed several times with water and ethanol, dried at 90 °C overnight and calcined at 300 °C for 2 hours (rate 2 °C/min).

*Synthesis of Au colloids.* Au colloids were prepared using two different techniques: (i) glucose reduction of Au(III) in alkaline water in presence of PVP as stabilizing agent and (ii) hydrogen reduction of Au(I) amido complex.

*Glucose reduction of Au(III).*[72] PVP (158 mg, 1.39 mmol) and NaOH (161 mg, 4.03 mmol) were dissolved in 90 ml of distilled water, the solution was heated under vigorous stirring at 95 °C. Once this temperature is reached, an aqueous solution (10 ml) of HAuCl₄·3H₂O (198 mg, 0.503 mmol) and β-D-glucose (181 mg, 1.01 mmol) were added to the flask quickly, and stirred for 2.5 minutes. After reaction, a deep red stable solution of Au NPs is obtained.

*Decomposition of Au(I) amido complex.* The synthetic procedure was carried out under a dry argon atmosphere and using anhydrous solvent. Typically, 10 mg (28 10⁻³ mmol) of Au(I) amido complex (see below for the synthesis) were dissolved in 25 ml of THF, then n-octylsilane (1 eq, 28 10⁻³ mmol, 4 mg) was added. The resulting solution was pressurized with 3 bar of H₂ and left under stirring overnight. After reaction the colorless solutions turned deep purple and a stable solution of AuNPs is obtained.

*Synthesis of {Au[N(SiMe₃)₂]}₄.* The synthesis of the Au(I) amido complex {Au[N(SiMe₃)₂]}₄ has been carried out starting directly from Lithium bis(trimethylsilyl)amide (commonly abbreviated as LiHMDS, Lithium HexaMethylDiSilazide) following the procedure reported in literature.[73] All the synthetic procedure were carried out under a dry argon atmosphere and under light exclusion, using anhydrous solvent. A solution of AuCl (0.69 g, 2.97 mmol) in diethylether (20 ml) was cooled at -78°C (CO2(s) in acetone) then a solution of LiHDMS (0.497 g, 2.97 mmol) in anhydrous diethylether (30 ml) has been added dropwise. The mixture was allowed to warm at RT on its own and was left stirred overnight, yielding a dark brown mixture. The solvent was removed and the product was extracted with 30 ml of pentane (the mixture was kept under vigorous stirring

for 2 hours and then the solution was filtered using a canula fitted with a filter paper). The volume of the solution was reduced just until some crystals started to appear then the product was crystallized over 5 days at -30°C. The solvent was removed through canula fitted with filter paper and the solid was dried under vacuum.

*Catalyst preparation.* Gold was deposited on the two considered $CeO_2$ supports, nanoparticulated and commercial, using two different methods: (i) immobilization of the preformed colloids, and (ii) deposition-precipitation. Different amounts of gold were loaded in the supports, 0.3, 0.5, 1 and 5 wt.%.

*Immobilization of preformed colloids* (**I**). The samples were prepared by impregnation of $CeO_2$ *via* an incipient wetness method using the colloids prepared by glucose reduction of Au(III). The catalyst were dried at 120 °C overnight and calcined at 300 °C for 2 h (rate 10 °C/min).

*Deposition precipitation*[26] (**DP**). The pH of a water solution of $HAuCl_4 \cdot 3H2O$, $1 \cdot 10^{-3}$ M, was adjusted to 8 by adding drop wise a 0.1 M aqueous NaOH solution. Similarly the pH of a water suspension (300 ml) of 2 g of $CeO_2$ was brought to 8. The gold solution was then added drop wise to the ceria suspension under vigorous stirring at room temperature and the stirring continued for 2 h at 65 °C, this results on the selective deposition of $Al(OH)_3$ on the surface of the metal oxide. The pH of the mixture was continuously monitored and kept at the fixed value of 8. The mixture was subjected to ultrasound treatment for 15 minutes in an ultrasonic bath. Then the solid was filtered, washed several times with water to remove chloride, dried at 110 °C overnight and calcined at 300 °C for 2 hours (rate 2°C/min).

Table 1 summarizes the prepared samples. The following abbreviations are used to identify the catalysts: Ce60 denotes the commercial $CeO_2$; hsCe denotes the high surface $CeO_2$, which may be followed by Cl or $NO_3$, depending on the precursor; I denotes immobilization; DP denotes deposition-precipitation; and finally the number (0.3, 0.5, 1, 5) denotes the gold loading (wt.%).

Table 1. List of the used abbreviations.

| Support | Impregnation(**I**)_Au loading wt.% | | | | Deposition-Precipitation(**DP**)_Au loading wt.% | | | |
|---|---|---|---|---|---|---|---|---|
| Ce60 | I_0.3 | I_0.5 | I_1 | I_5 | DP_0.3 | DP_0.5 | DP_1 | DP_5 |
| hsCe_Cl | | I_0.5 | | | | DP_0.5 | | |
| hsCe_NO$_3$ | | I_0.5 | | | | DP_0.5 | | |

*Catalytic tests.* The alcohols oxidation reactions were carried out in a magnetically stirred glass batch reactor (Figure 3) in presence of toluene as solvent at 100 °C, at

atmospheric pressure by bubbling air through the slurry (20 ml/min). Typically 180 mg of the catalyst were suspended in a toluene solution (10 ml) of 4.6 mmol of the alcohol and 4.6 mmol of 1,2,4-trimethylbenzene, chemically inert in the used conditions and added to correct the effect of the solvent stripping. The resulting mixture was heated at 100°C for 4 hours and air was bubbled continuously trough the suspension. After the reaction the catalyst was separated by centrifugation (1500 rpm for 10 minutes) and the products were analyzed by Carlo Erba 4300 gas chromatograph, equipped with FID and a HP-5 column (length 30 m, i.d. 0.32 mm, film width 0.25 μm) and identified by GC-MS analysis using an AgilentTechnology 6890N equipped with a 5973 mass selective detector and an HP5 column (length 25 m, i.d. 0.25 mm, film width 1.5 μm). Products concetration were calculated by GC analysis using undecane as internal standard.
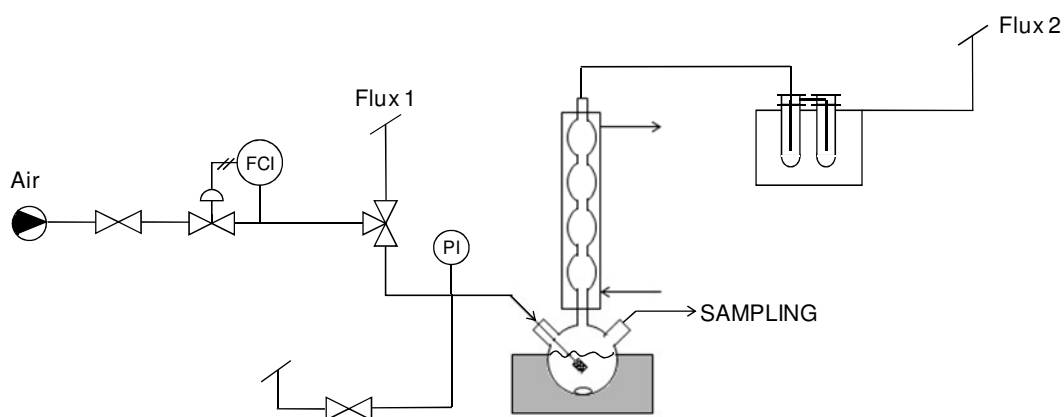


Figure 3. Schematic representation of the used plant.

*Characterizations.* Surface area were measured by $N_2$ sorption isotherms at -196 °C on a Sorpty 1750 CE apparatus and single point BET analysis methods, samples were pretreated under vacuum at 150 °C.

TEM images were recorded using a TEM/STEM FEI Tecnai F20 working at 200KeV. The crystal plane spaces, Fast Fourier Transform (FFT) rings and Inverse Fast Fourier Transform (IFFT) patterns were obtained through analyzing the TEM micrographs using the Gatan Digital Micrograph software. By the techniques of FFT, applying masks, invert FFT transform, data about crystal plane space were obtained, which is the base for the finding of crystal phases by comparing them with the standard ICDD-PDF data

# RESULTS AND DISCUSSIONS

The first part of the work deals with investigation of the activity of different gold supported on $CeO_2$ catalysts in the oxidation of benzyl alcohol to benzaldehyde. Tests were performed under very mild condition, using toluene as solvent, at 100°C and air at atmospheric pressure as oxidant (Scheme 1). In particular the influence of preparation procedure and effect of support particles size have been investigated.
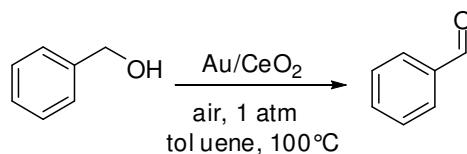


Scheme 1

Influence of the preparation procedure on the catalytic activity of supported gold nanoparticles has been investigated by preparing two series of catalysts with the same gold content (0.3-5 wt.%) and the same commercial support ($CeO_2$ VP 60, Ce60) using two different techniques:

- **DP** samples, prepared by deposition-precipitation
- **I** samples, prepared by colloids (glucose reduction of Au(III)) immobilization

Results of benzyl alcohol oxidation reactions are reported in Table 2 and are graphically summarized in Figure 4.

Table 2. Oxidation of benzyl alcohol catalyzed by two series (DP and I) of Au supported on commercial $CeO_2$ (Ce60) catalysts: effects of gold content and preparation procedure. [a]

| catalyst | conv (%) | yield (%) | | sel (%) | bal (%) | catalyst | conv (%) | yield (%) | | sel (%) | bal (%) |
|---|---|---|---|---|---|---|---|---|---|---|---|
| | | BA | BB | BA | | | | BA | BB | BA | |
| **Ce60_DP_0.3** | 32.2 | 26.6 | 1.4 | 83 | 87 | **Ce60_I_0.3** | 21.8 | 17.7 | 0.6 | 81 | 84 |
| **Ce60_DP_0.5** | 37.0 | 30.8 | 1.2 | 83 | 87 | **Ce60_I_0.5** | 23.6 | 19.4 | 0.5 | 82 | 85 |
| **Ce60_DP_1** | 39.7 | 30.9 | 2.1 | 78 | 83 | **Ce60_I_1** | 22.0 | 19.1 | 0.2 | 87 | 88 |
| **Ce60_DP_5** | 59.5 | 48.0 | 6.7 | 81 | 92 | | | | | | |

[a] Reaction conditions: toluene solution (10 ml) of 4.6 mmol benzyl alcohol, 4.6 mmol 1,2,4-trimethylbenzene, 180 mg catalyst, 100°C, air bubbling rate (20 ml/min, 1 atm). Conversion, yield, selectivity and balance values measured at t = 4 h. Abbreviations: benzaldehyde (BA) and benzylbenzoate (BB)
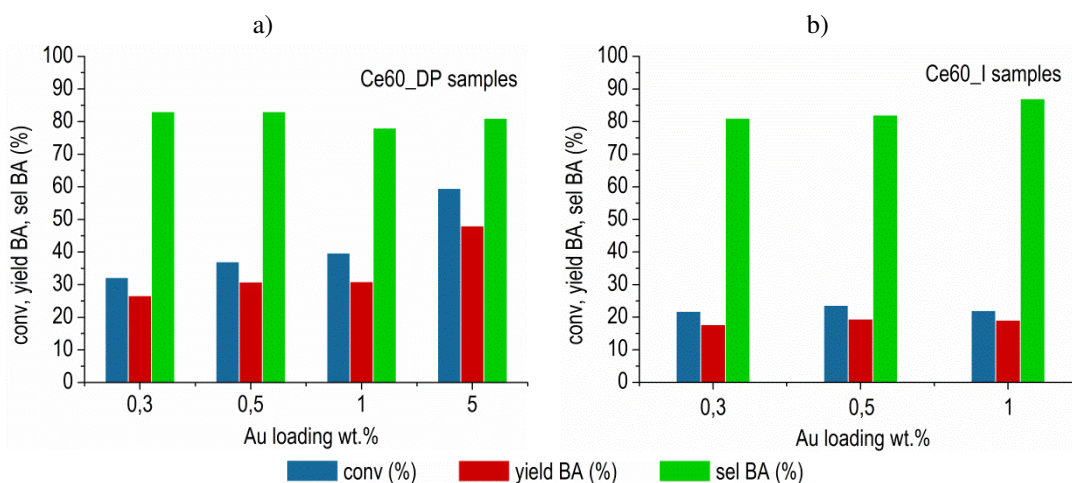
Figure 4. Graphical representation of the data reported in Table 2. Catalytic activity of two series of Au supported on commercial CeO$_2$ (Ce60) catalysts with different gold loading (0.3-0.5 wt.%) prepared with different techniques: a) deposition-precipitation (DP) and b) sol-immobilization (I). Conversion, yield, selectivity and balance values measured at t = 4 h. Abbreviation: benzaldehyde (BA).

Both the series of catalysts were active the oxidation of benzyl alcohol to the corresponding aldehyde using air as oxidant, furthermore in all tests benzylbenzoate was detected as the only side-product of the reaction, but the formation of hardly detectable amounts other by-products can not be excluded. It should be noted that reaction balances are always lower than 90 (except for Ce60_DP_5 sample). This is probably attributable both to the formation of not detected side-products, as already observed, and to some limitations directly correlated to the operating conditions and to the experimental setup. Experimental measurements of the changes in reactants and products concentration suffer from errors related to tendency for the solvent and for the reactants to move into the air flow. The correction factor calculated from the changes in concentration of an inert compound (1,2,4-trimethylbenzene) allowed us to reduce but not eliminate this error.

Results show that activities of the samples were influenced by synthetic procedure. Catalysts prepared by deposition-precipitation were more active respect the analogous ones prepared by colloids immobilization: the conversions of benzyl alcohol and the yields of benzaldehyde obtained for the former catalysts were considerably much higher (10%) respect those of the latter series. In order to rationalize the experimental relationship between activity and preparation procedure, we further investigated the properties of the synthesized materials, in particular metal particles size and was evaluated by TEM analysis.

The small difference in the scattering potentials of the gold and CeO$_2$ results in a relatively poor contrast, then Au nanoparticles are hardly visible. Despite these difficulties the presence of gold was confirmed by SAED analysis, and a carefully investigation of the TEM micrographs complemented with Fast Fourier Transform (FFT) diffractogram analysis show that nanoparticles made via sol-immobilization

(Figure 5b) are generally bigger (7-8 nm) than those obtained by deposition-precipitation (Figure 5a), which are around 2-4 nm.



a)                                                                           b)
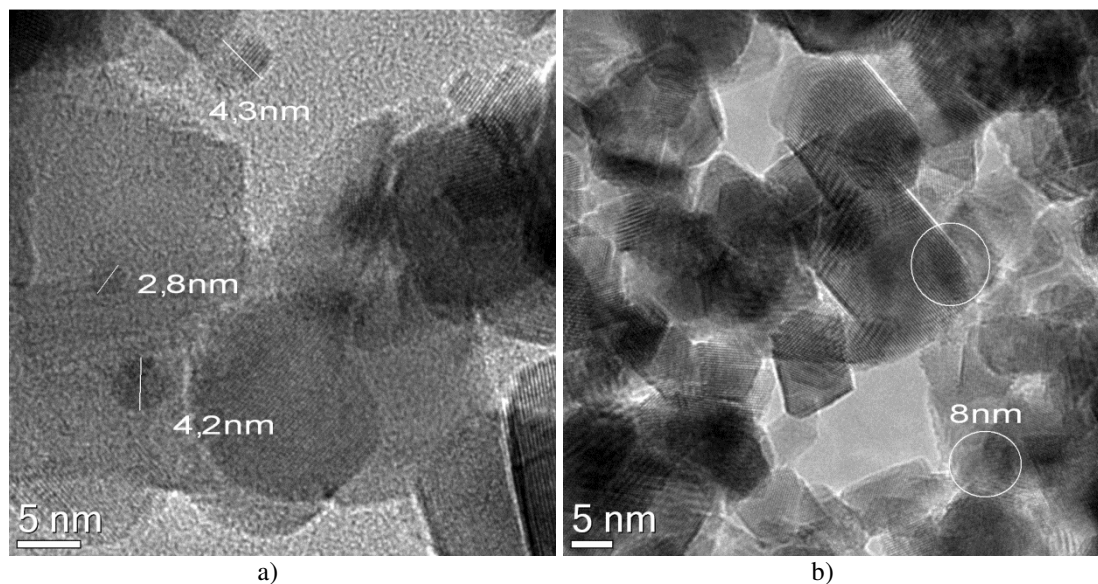
Figure 5. TEM micrographs of Au supported on commercial $CeO_2$ (0.5 wt.% Au) catalysts prepared by a) deposition-precipitation (Ce60_DP_0.5) and b) sol-immobilization (Ce60_I_0.5).

Thus, the higher activity of the DP samples may be ascribed to the smaller size of gold particles using this method. Moreover, activity of sol-immobilized Au/CeO₂ samples could be affected by the residual presence of organic species derived from PVP decomposition that may reduce or even prevent the accessibility to the catalytic sites.[74]

With respect to the gold loading (0.3-5 wt.%), the obtained data indicate that this parameter has only a slight effect on the reaction rate, this behavior may be probably ascribed to the predominantly effect of the particles dispersion. A reasonable explanation to justify this behavior relies on assuming that the amount of gold loaded on the support causes differences in particles dispersion, in particular increasing in the gold content favors the formation of aggregates, with a consequent reduction in the particles dispersion. Furthermore agglomeration of the particles results in the reduction of the number of both external gold atoms, and interface sites, which are mainly responsible for the catalytic activity. This latter hypothesis, was evaluated performing some tests under the substrate to gold molar ratio of 500 (0.2 mol% Au), then different amounts of catalyst were used (Table 3).

As expected, results show that gold dispersion plays a fundamental role in determining the catalyst activity, the sample with 0.5 wt.% of gold is significantly more active than the samples with higher gold content (1 and 5 wt.%). However, effect of gold loading on particles size can not be excluded, thus further TEM analysis are required.

Table 3. Oxidation of benzyl alcohol catalyzed by Au supported on commercial $CeO_2$ (Ce60) catalysts prepared by deposition-precipitation: effects of gold dispersion. [a]

| catalyst | amount of catalyst (mg) | conv (%) | yield (%) | | sel BA (%) | bal (%) |
|----------|------------------------|----------|-----------|-----------|------------|---------|
| | | | BA | BB | | |
| **Ce60_DP_0.5** | 360 | 51.9 | 44.2 | 2.8 | 85 | 91 |
| **Ce60_DP_1** | 180 | 39.7 | 30.9 | 2.1 | 78 | 83 |
| **Ce60_DP_5** | 36 | 18.9 | 16.9 | 0.3 | 90 | 91 |

Reaction conditions: toluene solution (10 ml) of 4.6 mmol benzyl alcohol, 4.6 mmol 1,2,4-trimethylbenzene, 100°C, air bubbling rate (20 ml/min, 1 atm), benzyl alcohol : Au = 500 mol/mol (0.2 mol% Au), Conversion, yield, selectivity and balance values measured at t = 4 h. Abbreviations: benzaldehyde (BA) and bensylbenzoate (BB)

Summarizing, catalyst 0.5 wt.% $Au/CeO_2$ exhibited the best catalytic performances, yielding 44.2% of benzaldehyde under tested conditions. In order to evaluate the possibility to enhance the activity of the catalyst by increasing surface of the support, as observed by Corma *et al.*[39], we proceeded with the synthesis of an high-surface $CeO_2$ following a surfactant-method. Different techniques, such as precipitation, sol-gel, hydrothermal synthesis, microemulsion and surfactant-method, have been successfully employed for the synthesis of nanocrystalline $CeO_2$ with surface area ranging from 100 to 600 $m^2/g$.[39,75–79] Process reported by Corma,[39] based on thermolysis of an acidified $Ce(NO_3)_4$ solution, required the set-up of a complex apparatus for the electrochemical oxidation of $Ce^{3+}$,[80] whereas an easier and versatile templated synthesis method suitable for nanocrystalline $CeO_2$ using $CeCl_3$ as precursor have been proposed by Guo *et al.*[63]

Based on this consideration we investigated the possibility to successfully prepare a high surface $CeO_2$ following a procedure similar to the one reported by Guo[63] using two different cerium precursor, $CeCl_3$ and $Ce(NO_3)_3$. The successfully use of the nitrate salt instead of the chloride, which is more expensive, hard to remove, and is known to be a poison for gold supported catalyst, represent the greatest advantages deriving from the use of this procedure. Calcination of the precipitated materials at 300 °C for 2 hours yielded hsCe_Cl and hsCe_NO3 (see the list of abbreviations above) as pale yellow powders, the BET surface area of these samples were found to be 222 and 220 $m^2/g$, respectively, owing to the small size of the particles. TEM micrographs of hsCe_Cl and commercial $CeO_2$ are reported in Figure 6a and Figure 6b, respectively. It can be seen that quasispherical $CeO_2$ particles of fairly uniform size, around 4 nm, have been obtained in case of high surface sample, whereas TEM image of commercial $CeO_2$ reveals bigger particles with irregular shapes.
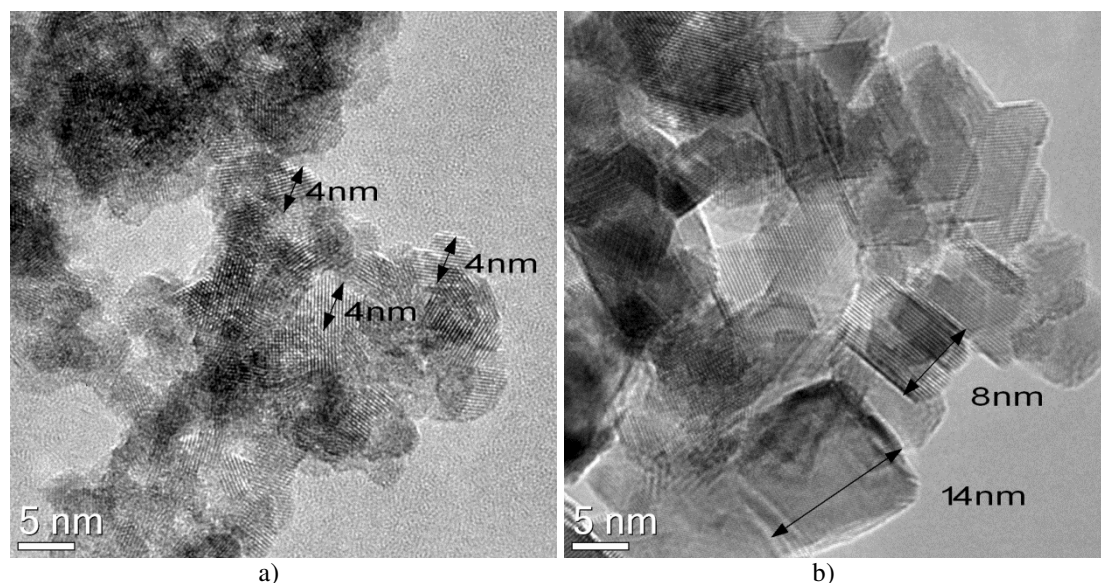
Figure 6. TEM micrographs of a) high surface area $CeO_2$ prepared by $CeCl_3 \cdot 7H_2O$ (hsCe_Cl) and b) commercial $CeO_2$ (Ce60).

Then four catalysts with the same gold loading as the most active sample previously founded, 0.5 wt%, were prepared using both deposition-precipitation and sol-immobilization methods and were tested in benzyl alcohol oxidation. Table 4 and Figure **7** report the catalytic activities of Au/hsCe samples in the oxidation of benzyl alcohol, compared to the ones of Au/Ce60.

Table 4. Benzyl alcohol oxidation catalyzed by Au supported on high surface area $CeO_2$ (hsCeCl and hsCeNO$_3$) and on commercial $CeO_2$ (Ce60): effect of the particles size of the support and preparation procedures. [a]

| catalyst | conv (%) | yield (%) | | sel BA (%) | bal |
|---|---|---|---|---|---|
| | | BA | BB | | |
| **hsCeCl_I_0.5** | 31.7 | 24.5 | 1.1 | 78 | 81 |
| **hsCeNO$_3$_I_0.5** | 34.1 | 25.7 | 1.2 | 75 | 79 |
| **Ce60_I_0.5** | 22.0 | 19.1 | 0.2 | 87 | 88 |
| **hsCeCl_DP_0.5** | 64.9 | 47.8 | 8.5 | 74 | 87 |
| **hsCeNO$_3$_DP_0.5** | 57.0 | 39.1 | 3.8 | 69 | 75 |
| **Ce60_DP_0.5** | 37.0 | 30.8 | 1.2 | 83 | 87 |

Reaction conditions: toluene solution (10 ml) of 4.6 mmol benzyl alcohol, 4.6 mmol 1,2,4-trimethylbenzene, 180 mg catalyst (Au loading 0.5 wt.%), 100°C, air bubbling rate (20 ml/min, 1 atm). Conversion, yield, selectivity and balance values measured at t = 4 h. Abbreviations: benzaldehyde (BA) and benzylbenzoate (BB)
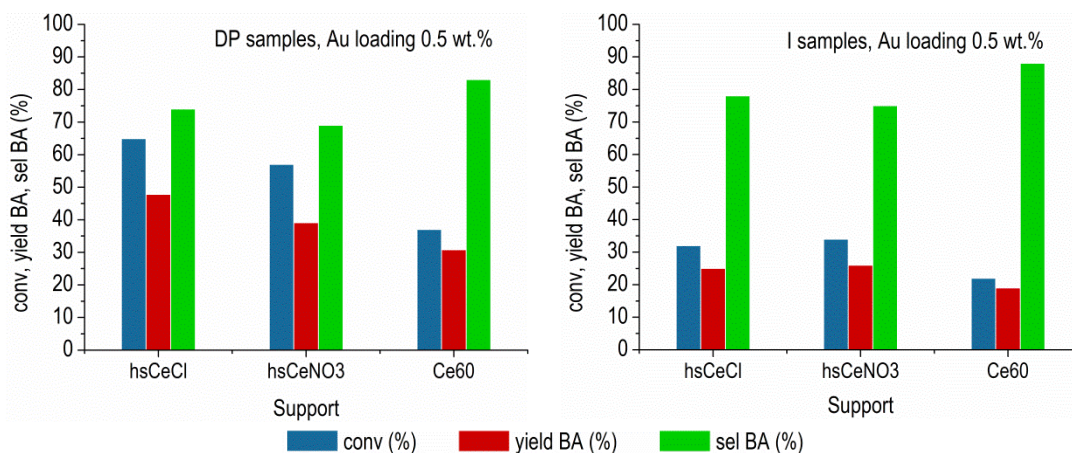
Figure 7. Graphical representation of the data reported in Table 4. Benzyl alcohol oxidation catalyzed by two series of Au supported on high surface area $CeO_2$ (hsCeCl and hsCeNO$_3$) and on commercial $CeO_2$ (Ce60) prepared with two different techniques: a) deposition-precipitation and b) sol-imobilization.

Conversion, yield, selectivity and balance values measured at t = 4 h. Abbreviation: benzaldehyde (BA).

Data show that properties of the support have been drastically changed by decreasing the size of the particles: the reduction of the $CeO_2$ particles size provide a significant improvement of the catalytic performances of the Au supported on CeO2 catalysts compared to those prepared on commercial $CeO_2$ ($S_{BET}$ = 60 m$^2$/g). The effect of the particle size of the support is much more evident in case of DP-samples, conversion increase from 37 to 64.5%, whereas in case sol-immobilized Au/hsCeO$_2$ only a slight increment of about 10% is observed. The effect of the particle size of the support is more efficiently when the size of the gold and $CeO_2$ particles are comparable, as in case of DP-samples. Gold nanoparticles obtained by DP supported on high surface area $CeO_2$ are very hardly visualized by TEM, due to the fact that dimensions of both gold and $CeO_2$ particles are in the range of only few nanometers. Although, combination of TEM imaging and SAED Figure 8 showed that depostition-precipitation on high surface area $CeO_2$ resulted in the formation of very small Au nanoparticles of 1-2 nm together with subnanometric gold nanoparticles. Finally, as already observed in case of commercial $CeO_2$, DP-samples showed superior performances in terms of higher conversions and yields in benzaldehyde respect to the analogous ones prepared by immobilization.
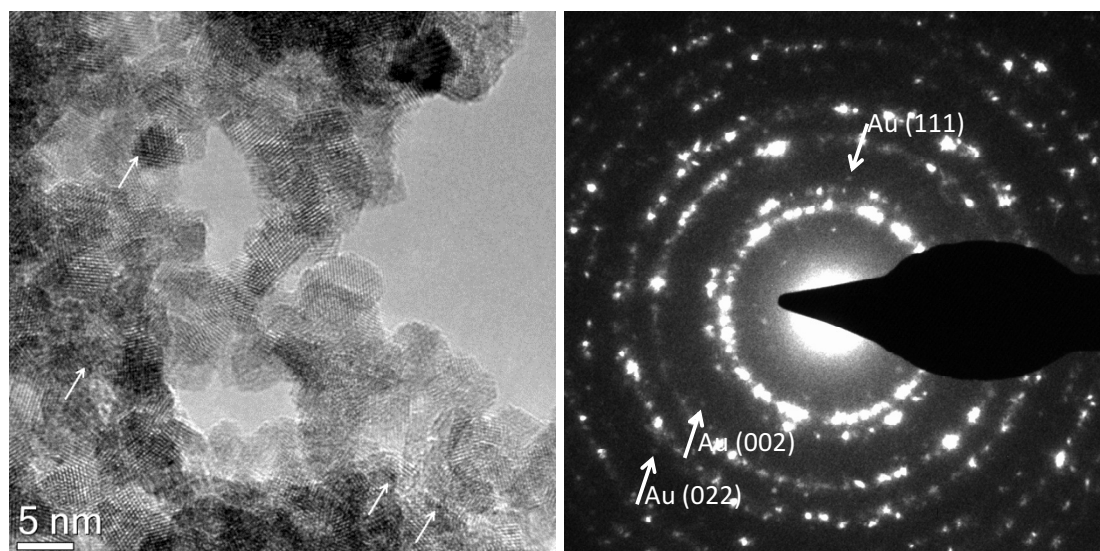
Figure 8. TEM image of Au/hsCeCl, and relative SAED

The second part of the work focused on the final goal of the study: the oxidation of piperonyl alcohol to piperonal (Scheme 2) under very mild conditions: 100°C, atmospheric air as oxidant and toluene as solvent.
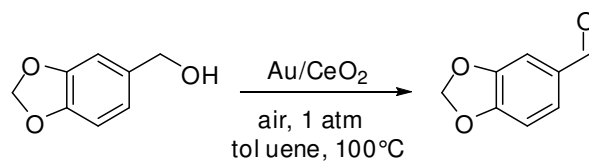


Scheme 2

The most active sample for each series of previously prepared catalysts were tested in piperonyl alcohol oxidation. The catalytic performances of the selected catalysts are reported in Figure 9.
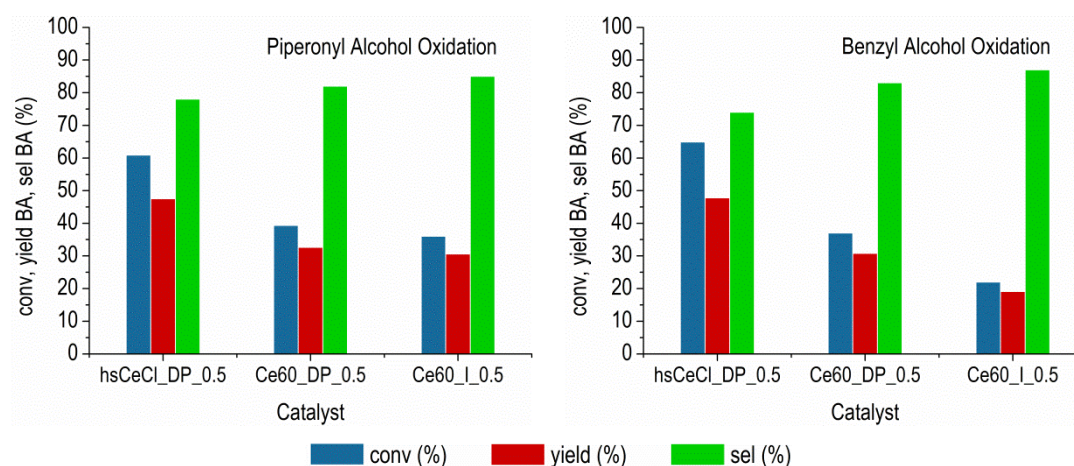


Figure 9. Graphical representation of the results of the piperonyl alcohol oxidation (left) and benzyl alcohol oxidation (right) catalyzed by different Au supported on $CeO_2$ samples (Au content 0.5 wt. %) Conversion, yield, selectivity and balance values measured at t = 4 h.

As can be seen from the above reported results the activity of the samples followed a similar trend to that observed in benzyl alcohol oxidation. Gold supported on the high surface area $CeO_2$ sample prepared by deposition-precipitation (hsCeCl_DP_0.5) exhibited the highest activity being the most active catalyst. In all tests piperonal has been detected as only product of the reaction, but selectivity values suggest that some by-products in hardly detectable amounts were probably produced. Moreover limitations related to the experimental setup, as already described in case of benzyl alcohol, resulted in a general underestimation of both conversions and yields.

Finally, in the last part of the work we developed a novel and simple procedure for the synthesis Au colloids without the use of tricky stabilizing agents, such as PVP, which are known to reduce the activity of the catalyst. In particular we investigated the possibility to synthesize gold colloids *via* one pot decomposition of $\{Au[N(SiMe_3)_2]\}_4$, in presence of n-octylsilane,. This complex has been successfully used for the synthesis of Au NPs on passivated silica.

The procedure started with the synthesis of the $\{Au[N(SiMe_3)_2]\}_4$, the most difficult step which requires high purity degree of the reactants and an accurate control of the reaction conditions, since most of reagents and products are highly air, moisture and light sensitive. Despite these difficulties , we managed to obtain the gold (I) amido complex in 10% yield by reacting AuCl with Lithium bis(trimethylsilyl)amide (LiHMDS) in diethyl ether, Scheme 3.
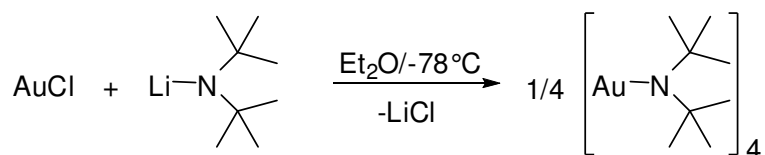


Scheme 3

Then the mild reduction of the Au(I) complex under $H_2$ led to the efficient formation of monodispersed nanoparticles with a narrowed size distribution centered at 3.5 nm, as shown by TEM micrographs and particles size distribution in Figure 10. Due to the small size of the particles, this octylsilane-stabilized colloid solution represent a very promising starting material for the synthesis of supported gold catalyst. Further studies on the possibility to efficiently support this nanoparticles on $CeO_2$ by simple sol immobilization are needed, moreover the stability of the prepared solution should be also investigated.
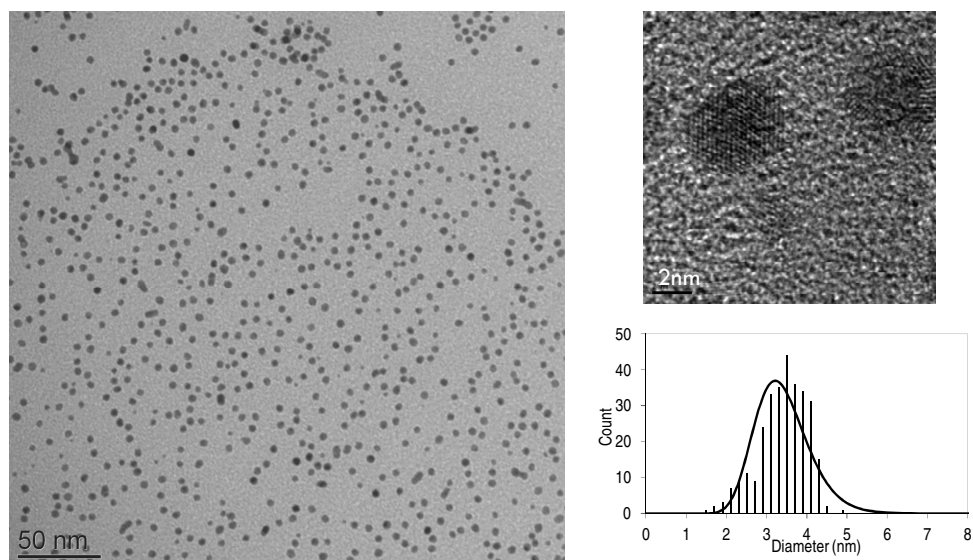
Figure 10. TEM and HRTEM images of colloids prepared by decomposition of the Au(I) amido complex, and relative particle size distribution.

# CONCLUSIONS

Benzaldehyde and piperonal, two aromatic substrates widely used as intermediates in the fine chemical industry, has been successfully prepared *via* direct liquid phase oxidation under mild condition of the corresponding alcohols catalyzed by Au/CeO$_2$. Various gold supported on ceria catalysts were synthesized *via* deposition-precipitation and immobilization of colloids, prepared by glucose reduction of Au(III) in presence of PVP. The synthesized catalysts were found to be active in the in absence of a base and using atmospheric air as oxidant, conditions under which most of the catalysts are inactive.

Deposition-precipitation samples were found to more active respect the analogous ones prepared by sol-immobilization. The higher activity has been attribute to the smaller particle sizes and to the absence of any sticky ligands, such as PVP. Marked improvement in the activity have been observed by increasing the surface area of the support, reduction of crystallite size in the region of few nanometers resulted in an enhancement of the synergic effect between CeO$_2$ and gold.

Furthermore promising results have been obtained in the development of a new and simple procedure for the synthesis of small colloids *via* one pot decomposition of Au(I) amido complex, we will further investigate the possibility to successfully immobilize these nanoparticles on CeO$_2$.

# REFERENCES

(1)     Bond, G. C.; Sermon, P. A.; Webb, G.; Buchanan, D. A.; Wells, P. B. *J. Chem. Soc., Chem. Commun.* **1973**, 444-445.

(2)     Haruta, M.; Kobayashi, T.; Sano, H.; Yamada, N. *Chem. Lett.* **1987**, *16*, 405-408.

(3)     Haruta, M.; Yamada, N.; Kobayashi, T.; Iijima, S. *J. Catal.* **1989**, *115*, 301-309.

(4)     Hutchings, G. J. *J. Catal.* **1985**, *96*, 292-295.

(5)     Hashmi, A. S. K.; Hutchings, G. J. *Angew. Chem., Int. Ed.* **2006**, *45*, 7896-7936.

(6)     Taylor, P.; Bond, G. C.; Thompson, D. T. *Catal. Rev.: Sci. Eng.* **1999**, *41*, 319-388.

(7)     Corma, A.; Garcia, H. *Chem. Soc. Rev.* **2008**, *37*, 2096-126.

(8)     Hvolbæk, B.; Janssens, T. V. W.; Clausen, B. S.; Falsig, H.; Christensen, C. H.; Nørskov, J. K. *Nano Today* **2007**, *2*, 14-18.

(9)     Pyykko, P. *Angew. Chem., Int. Ed.* **2002**, *41*, 3573-3578.

(10)    Bond, G. C. *Catal. Today* **2002**, *72*, 5-9.

(11)    Bond, G. C. *J. Mol. Catal. A: Chem.* **2000**, *156*, 1-20.

(12)    Meyer, R.; Lemire, C.; Shaikhutdinov, S. K.; Freund, H.-J. *Gold Bull.* **2004**, *37*, 72-124.

(13)    Lopez, N. *J. Catal.* **2004**, *223*, 232-235.

(14)    Haruta, M.; Daté, M. *Appl. Catal., A* **2001**, *222*, 427-437.

(15)    Gluhoi, A. C.; Bogdanchikova, N.; Nieuwenhuys, B. E. *J. Catal.* **2005**, *232*, 96-101.

(16)    Ma, Z.; Dai, S. *Nano Res.* **2010**, *4*, 3-32.

(17)    Haruta, M. *Catal. Today* **1997**, *36*, 153-166.

(18)    Grisel, R. J. H.; Nieuwenhuys, B. E. *J. Catal.* **2001**, *199*, 48-59.

(19)    Pushkarev, V. V.; Kovalchuk, V. I.; D'Itri, J. L. *J. Phys. Chem. B* **2004**, *108*, 5341-5348.

(20)    Campbell, C. T.; Peden, C. H. F. *Science* **2005**, *309*, 713-714.

(21)    Esch, F.; Fabris, S.; Zhou, L.; Montini, T.; Africh, C.; Fornasiero, P.; Comelli, G.; Rosei, R. *Science* **2005**, *309*, 752-755.

(22)    Kim, H. Y.; Lee, H. M.; Henkelman, G. *J. Am. Chem. Soc.* **2012**, *134*, 1560-1570.

(23)    Trovarelli, A. *Catal. Rev.: Sci. Eng.* **1996**, *38*, 439-520.

(24)    Laachir, A.; Perrichon, V.; Badri, A.; Lamotte, J.; Catherine, E.; Lavalley, J. C.; Quéméré, E.; Sauvion, G. N.; Touret, O. *J. Chem. Soc., Faraday Trans.* **1991**, *87*, 1601-1609.

(25)    Manzoli, M.; Boccuzzi, F.; Chiorino, a; Vindigni, F.; Deng, W.; Flytzanistephanopoulos, M. *J. Catal.* **2007**, *245*, 308-315.

(26)    Pillai, U. R.; Deevi, S. *Appl. Catal., A* **2006**, *299*, 266-273.

(27)    Guzman, J.; Carrettin, S.; Corma, A. *J. Am. Chem. Soc.* **2005**, *127*, 3286-7.

(28)    Fierro Gonzalez, J. C.; Gates, B. C. *J. Phys. Chem. B* **2004**, *108*, 16999.

(29)    Guzman, J.; Kuba, S.; Fierro-Gonzalez, J. C.; Gates, B. C. *Catal. Lett.* **2004**, *95*, 77-86.

(30)    Concepción, P.; Carrettin, S.; Corma, A. *Appl. Catal., A* **2006**, *307*, 42-45.

(31)    Chen, M. S.; Goodman, D. W. *Science* **2004**, *306*, 252-255.

(32)    Bera, P.; Hegde, M. S. *Catal. Lett.* **2002**, *79*, 75-81.

(33)    Centeno, M. A.; Paulis, M.; Montes, M.; Odriozola, J. A. *Appl. Catal., A* **2002**, *234*, 65.

(34)    Guzman, J.; Gates, B. C. *J. Am. Chem. Soc.* **2004**, 2672-2673.

(35)    Venezia, A. M.; Pantaleo, G.; Longo, A.; Di Carlo, G.; Casaletto, M. P.; Liotta, F. L.; Deganello, G. *J. Phys. Chem. B* **2005**, *109*, 2821-2827.

(36)    Moreau, F.; Bond, G. C. *Catal. Today* **2007**, *122*, 215-221.

(37)    Pietron, J. J.; Stroud, R. M.; Rolison, D. R. *Nano Lett.* **2002**, *2*, 545-549.

(38)    Rolison, D. R. *Science* **2003**, *299*, 1698-1701.

(39)    Carrettin, S.; Concepción, P.; Corma, A.; López Nieto, J. M.; Puntes, V. F. *Angew. Chem., Int. Ed.* **2004**, *43*, 2538-2540.

(40)    Guan, Y.; Ligthart, D. a. J. M.; Pirgon-Galin, Ö.; Pieterse, J. A. Z.; Santen, R. a.; Hensen, E. J. M. *Top. Catal.* **2011**, *54*, 424-438.

(41)    Huang, X.-S.; Sun, H.; Wang, L.-C.; Liu, Y.-M.; Fan, K.-N.; Cao, Y. *Appl. Catal., B* **2009**, *90*, 224-232.

(42)    Lu, J.-L.; Gao, H.-J.; Shaikhutdinov, S.; Freund, H.-J. *Catal. Lett.* **2007**, *114*, 8-16.

(43)    Abad, A.; Concepción, P.; Corma, A.; García, H. *Angew. Chem., Int. Ed.* **2005**, *44*, 4066-4069.

(44)    Haruta, M. *CATTECH* **2002**, *6*, 102-115.

(45)    Gluhoi, A. C.; Dekkers, M. A. P.; Nieuwenhuys, B. E. *J. Catal.* **2003**, *219*, 197-205.

(46)    Lee, S.-J.; Gavriilidis, A. *J. Catal.* **2002**, *206*, 305-313.

(47)    Moreau, F.; Bond, G. C. *Appl. Catal., A* **2006**, *302*, 110-117.

(48)    Chang, C.-K.; Chen, Y.-J.; Yeh, C.-T. *Appl. Catal., A* **1998**, *174*, 13-23.

(49)    Bonelli, R. Cluster–derived Gold/Iron catalysts for environmental applications, University of Bologna, 2010.

(50)    Prasad, B. L. V.; Stoeva, S. I.; Sorensen, C. M.; Klabunde, K. J. *Chem. Mater.* **2003**, *15*, 935-942.

(51)    Blosi, M.; Albonetti, S.; Dondi, M.; Baldi, G.; Barzanti, A.; Bitossi, M. *Process for preparing stable suspensions of metal nanoparticles and the stable colloidal suspensions obtained thereby,* WO Patent 2010/100107 A2 2010.

(52)    Pelzer, K.; Laleu, B.; Lefebvre, F.; Philippot, K.; Chaudret, B.; Candy, J. P.; Basset, J. M. *Chem. Mater.* **2004**, *16*, 4937-4941.

(53)    Gajan, D.; Guillois, K.; Delichère, P.; Basset, J.-M.; Candy, J.-P.; Caps, V.; Copéret, C.; Lesage, A.; Emsley, L. *J. Am. Chem. Soc.* **2009**, 14667-14669.

(54)    Sheldon, R. A.; Kochi, J. K. *Metal-Catalyzed Oxidations of Organic Compounds*; Academic Press: New York, 1981.

(55)    Prati, L.; Rossi, M. *J. Catal.* **1998**, *176*, 552-560.

(56)    Biella, S.; Prati, L.; Rossi, M. *J. Catal.* **2002**, *206*, 242-247.

(57)    Comotti, M.; Della Pina, C.; Matarrese, R.; Rossi, M. *Angew. Chem., Int. Ed.* **2004**, *43*, 5812-5815.

(58)    Abad, A.; Almela, C.; Corma, A.; García, H. *Tetrahedron* **2006**, *62*, 6666-6672.

(59)    Mori, K.; Hara, T.; Mizugaki, T.; Ebitani, K.; Kaneda, K. *J. Am. Chem. Soc.* **2004**, *126*, 10657-66.

(60)    Abad, A.; Corma, A.; García, H. *Chem.-Eur. J.* **2008**, *14*, 212-22.

(61)    Alhumaimess, M.; Lin, Z.; Weng, W.; Dimitratos, N.; Dummer, N. F.; Taylor, S. H.; Bartley, J. K.; Kiely, C. J.; Hutchings, G. J. *ChemSusChem* **2012**, *5*, 125-131.

(62)    Su, F.-Z.; Liu, Y.-M.; Wang, L.-C.; Cao, Y.; He, H.-Y.; Fan, K.-N. *Angew. Chem.* **2008**, *120*, 340-343.

(63)    Guo, M.-N.; Guo, C.-X.; Jin, L.-Y.; Wang, Y.-J.; Lu, J.-Q.; Luo, M.-F. *Mater. Lett.* **2010**, *64*, 1638-1640.

(64)    Opgrande, J. L.; Brown, E.; Hesser, M.; Andrews, J. Benzaldehyde. Kirk-Othmer Encyclopedia of Chemical Technology, John Wiley & Sons, Inc. 2003

(65)    Zviely, M. Aroma Chemicals. Kirk-Othmer Encyclopedia of Chemical Technology, John Wiley & Sons, Inc 2002.

(66)    Mais, H. E. *Process for producing aromatic aldehyde,* US 3,799,940 1974.

(67)    Corporation, Interchemical *Producing carbonyl compounds by ozonization-reduction process,* GB Patent 1,092,615 1967.

(68)    Farinacci, N. T. *Oxidation of organic compounds with a chromic oxidizing agent,* US Patent 2,794,813 1957.

(69)    Mitsui Toatsu Chemicals, *Procédé de préparation du pipéronal à partir du méthyléne dioxy-1,2 benzène et d'un N-alcoyl-formanilide,* FR Patent 2,412,541 1979.

(70)    Nakatani, K.; Inoue, T.; Nishizawa, T.; S., N.; Ishii, T. *Process for preparing piperonal,* US Patent 4,157,333 1979.

(71)    Borzatta, V.; Capparelli, E.; Gobbi, C.; Poluzzi, E. Process for synthesis of heliotropine and its derivatives WO Patent 2005/042512 (A1) 2005.

(72)    Pasini, T.; Piccinini, M.; Blosi, M.; Bonelli, R.; Albonetti, S.; Dimitratos, N.; Lopez-Sanchez, J. A.; Sankar, M.; He, Q.; Kiely, C. J.; Hutchings, G. J.; Cavani, F. *Green Chem.* **2011**, *13*, 2091-2099.

(73)    Bunge, S. D.; Just, O.; Rees, W. S. *Angew. Chem., Int. Ed.* **2000**, 3082-3084.

(74)    Quintanilla, A.; Butselaar-Orthlieb, V. C. L.; Kwakernaak, C.; Sloof, W. G.; Kreutzer, M. T.; Kapteijn, F. *J. Catal.* **2010**, *271*, 104-114.

(75)    Lee, J.-S.; Choi, S.-C. *Mater. Lett.* **2004**, *58*, 390-393.

(76)    Liang, X.; Xiao, J.; Chen, B.; Li, Y. *Inorg. Chem.* **2010**, *49*, 8188-90.

(77)    Djuričić, B.; Pickering, S. *J. Eur. Ceram. Soc.* **1999**, *19*, 1925-1934.

(78)    Terribile, D.; Trovarelli, A.; de Leitenburg, C.; Dolcetti, G.; Llorca, J. *Chem. Mater.* **1997**, *9*, 2676-2678.

(79)    Terribile, D.; Trovarelli, A.; Llorca, J.; de Leitenburg, C.; Dolcetti, G. *J. Catal.* **1998**, *178*, 299-308.

(80)    Chane-Ching, J. Y. Nouveau composé de cérium IV et son procédé de preparation, EP 0,208,580 (B1) 1987.